https://doi.org/10.5194/egusphere-2025-4830
Preprint. Discussion started: 7 October 2025

Comparative study of Low-grade metamorphic Precambrian supracrustal rocks and HP–UHP Rocks in the South Altyn Tagh: Insights into subduction-exhumation

Tuo Ma [a*], YongSheng Gai [a], Xiaoying Liao [a]

[a] State Key Laboratory of Continental Evolution and Early Life, Department of Geology, Northwest University, Xi'an 710069, China

*** Corresponding authors**

E-mail address: matuo12@163.com (T Ma)

Abstract

Low-grade metamorphic (LGM) rocks are widespread in high- to ultrahigh-pressure (HP–UHP) subduction zone yet frequently neglected in orogenic evolution. Establishing their spatiotemporal relationship with HP–UHP rocks and comparing protolith affinities are key to deciphering subduction zone architecture and exhumation dynamics. Here we investigate LGM Precambrian supracrustal rocks in the South Altyn Tagh (SAT) through field investigations, chronology and geochemical analysis, and comparison with HP–UHP rocks. Granites emplaced at 933–898 Ma, exhibiting crustal melting and syncollisional granite affinities, serving as robust markers for Rodinia convergence, consistent with protolith of regional HP–UHP granitic gneiss. Mafic dyke emplaced at ~806 Ma, exhibiting within-plate basalt (WPB) affinities, serving as markers for regime transition from collision to extension, consistent with protolith of regional eclogite and garnet pyroxenite. (Meta-)sedimentary rocks deposited during 939–932 Ma, exhibiting Taxidaban Group (Central Altyn block, CAB) affinities. Results reveal these LGM rocks lack significant Cambrian metamorphic (HP–UHP) overprinting but share protolith ages and characteristics with HP–UHP units, indicating shared formation origins yet distinct pre-subduction tectonic affiliations. This comparison implies that these supracrustal rocks may represent the non-subducted overlying plate of the SAT Early

https://doi.org/10.5194/egusphere-2025-4830
Preprint. Discussion started: 7 October 2025

Paleozoic subduction zone. Synthesizing our data with existing metamorphic records, we propose that the current spatiotemporal distribution of LGM and HP–UHP rocks in the SAT resulted from: (1) Early Paleozoic whole-slab continental subduction, followed by (2) differential exhumation and late-stage modification.

Key words: Low-grade metamorphic rock; South Altyn; Overall subduction; Differential exhumation

1. Introduction

Continental subduction zones are characterized by voluminous ortho- and para-gneisses of terrigenous origin enclosing minor mafic (eclogites, mafic granulites...) lenseses (Maruyama et al., 1996; Ernst, 2006). A prevailing hypothesis suggests that the entire continental slab—including both ortho-/para-gneisses and their enclosed eclogites—underwent consistent deep subduction and exhumation (Chopin et al., 2003; Haker et al., 2000; Andersen et al., 2010; Young & Kylander-Clark, 2015). However, HP–UHP signatures are predominantly preserved in rare eclogites or granulites, whereas the widely exposed gneisses/schists typically record only LGM mineral assemblages (Štípská et al., 2006; Whitney et al., 2008; Massonne, 2012; Li et al., 2020). This pronounced metamorphic disparity has constituted a pivotal scientific question and long-standing debate since the early continental deep subduction research (Proyer, 2003; Liu et al., 2013; Brueckner, 2018; Cao et al.， 2020). The current research bottleneck lies in distinguishing whether the LGM rocks either: (a) underwent deep subduction but failed to develop (or preserve) HP–UHP metamorphic records due to retrograde overprinting (Peterman et al., 2009; Palin et al., 2017), or (b) were never deeply subducted and are merely tectonically juxtaposed or intermingled with HP–UHP rocks (Yin et al., 2007; Sizova et al., 2012; Zhou et al., 2020). Resolving these issues would not only elucidate the genetic relationships between LGM and HP–UHP rocks, but also provide critical constraints on the formation and exhumation mechanisms of HP–UHP rocks, and the material sources and nature of subducted continental crust.

https://doi.org/10.5194/egusphere-2025-4830
Preprint. Discussion started: 7 October 2025

The SAT was widely recognized as a typical deep to ultra-deep continental subduction zone located in northwestern China (Liu et al., 2007, 2018; Gai et al., 2017). Extensive studies of the SAT have revealed multi-stages metamorphic evolution, comprising: (1) late Cambrian eclogite-facies metamorphism under a low thermal gradient (low dT/dP) (Liu et al., 2012; Ma et al., 2022), (2) contemporaneous high-pressure granulite-facies metamorphism under a high thermal gradient (high dT/dP) in thickened lower crust, and (3) Early to Middle Ordovician high-temperature to ultrahigh-temperature (HT–UHT) granulite- to amphibolite-facies overprinting (Zhang et al., 2017; Dong et al., 2021; Gai et al., 2022a,b). However, recent studies on the SAT metamorphic rocks have predominantly focused on the rock assemblages of high-pressure to ultrahigh-pressure (HP–UHP) units and their extreme metamorphic conditions, while neglecting systematic investigations of the widely distributed LGM rocks, particularly lacking critical understanding regarding their tectonic relationships with HP–UHP rocks and protolith correlations. These knowledge gaps conduced persistent uncertainties in SAT subduction zone architecture, including: (1) Whether LGM rocks underwent the continental deep-subduction process; (2) Can LGM rocks represent the overlying plate material; and (3) Compositional consistency between underthrust plate and overlying plate. Such fundamental questions further constrain our interpretation of the subduction–exhumation dynamics of the SAT.

This study focuses on the Precambrian supracrustal rocks in the SAT, conducting comprehensive investigations including spatial distribution mapping, protolith dating, detrital zircon age spectrum and protolith analysis, and comparation with HP–UHP rocks. The results demonstrate that these LGM rocks show no significant Cambrian metamorphic overprint, yet share consistent formation ages and characteristics with HP–UHP rocks (protolith). This suggests their common geological affinity during rock formation, but they may belonged to distinct tectonic units prior to Early Paleozoic continental deep subduction. Integrating our findings with previous research on various SAT metamorphic rocks, this study systematically reviews the genetic attributes of reported LGM and HP–UHP rocks in the region. We propose that the SAT continental slab likely underwent consistent subduction during the Early Paleozoic, but partitioned exhumation and modification during late orogenic stages, ultimately leading to the present-day spatial-temporal distribution pattern of metamorphic rocks with varying grades.

https://doi.org/10.5194/egusphere-2025-4830
Preprint. Discussion started: 7 October 2025

2. Geological backgrounds

The Altyn orogen exhibits a triangular NE–SW-trending architecture (Fig. 1a), comprising four distinct tectonic units (from north to south): the North Altyn Tagh (Unit I), the North Altyn subduction-accretion belt (Unit II), the Central Altyn block (Unit III), the South Altyn subduction-collision belt (Unit IV, SAT) (Fig. 1b).

Unit I was dominated by Archean-Proterozoic metamorphic basement (3.7-1.85 Ga) with tonalite-trondhjemite-granodiorite gneiss (TTG) gneisses, paragneisses, granitic veins and mafic intrusives (Gehrels et a1., 2003a, b; Lu et al., 2008; Ge et al., 2018), and considered as part of the Tarim Craton (RGXR, 1993).

Unit II was composed of supra-subduction zone (SSZ)-type ophiolitic mélanges (520–480 Ma) (Liu, 1999), LT–HP blueschist and eclogite (520–491 Ma) (Zhang et al., 2007; Liu et al., 2023), flysch sediments, and magmatic rocks (520–400 Ma) (Wu et al., 2007; Meng et al., 2017; Wang et al., 2019), and interpreted as an early Paleozoic accretionary orogenic system (Zhang et al., 2015).

Unit III was mainly consist of Meso- to Neoproterozoic metasedimentary and volcanic successions, including the Changcheng System (Bashikuergan Group; Ch), Jixian System (Taxidaban Group; Jx) and Qingbaikou System (Suoerkuli Group; Qb) (RGXR, 1993; RGGX, 2003). The Bashikuergan Group forms the metamorphic basement, featuring Mesoproterozoic sandstones, marbles, weakly metamorphic phyllites and schists, overlain by thick carbonate sequences (Jinyanshan Group; Jx). The Taxidaban Group comprises two formations: the Muzisayi Formation (Jxm) at the base and the overlying Jinyanshan Formation (Jxj), both exhibiting greenschist-facies metamorphism. The Jxm consists of sericite-quartz schist, phyllite, and quartzite at its base, transitioning upward into tuffaceous silt killas, calcareous/sandy killas, and minor sandy/pelitic/dolomitic intraclastic limestone; the Jxj is dominated by a carbonate sequence. The Suoerkuli Group is defined as a stratigraphic series with: clastic rocks intercalated with carbonates at the base; carbonate-dominated strata with clastic interbeds in the middle; and predominantly clastic rocks in the upper section. This group unconformably overlies the Taxidaban Group and is itself unconformably

https://doi.org/10.5194/egusphere-2025-4830
Preprint. Discussion started: 7 October 2025

overlain by the Lower Ordovician Elantage Formation. Detrital zircon U-Pb ages (1.3–1.2 Ga) constrain the depositional age, with intrusive 930 ± 10 Ma rhyolites and 922 ± 6 Ma granites (Gehrels et al., 2003b) indicating a pre-Neoproterozoic origin.

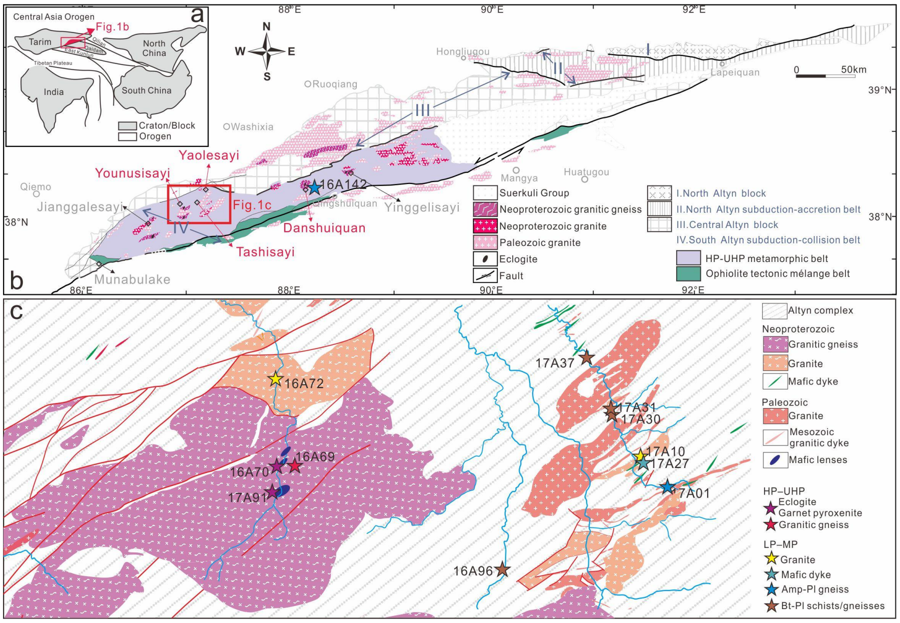

Fig.1. (a) Simplified tectonic framework of the Altyn orogen; (b) Geological overview of the Altyn orogen; (c) Simplified geological map shows the sample location in the study region.

Unit IV comprises two formations, the ophiolite tectonic mélange belt and SAT HP-UHP belt (Fig. 1b), that preserves Rodina supercontinent assembly (Liu et al., 2012; Wang et al., 2013) and Proto-Tethys Ocean evolution records (Liu et al., 1998; Kang, 2014; Yao et al., 2021). The SAT HP-UHP belt, also termed the Altyn Complex, is predominantly composed of Ky/Grt granitic gneisses with subordinate Ky/Grt paragneisses, intercalated with eclogites, garnet peridotites, garnet pyroxenites, and garnet amphibolite lenses (Liu et al., 2012; Wang et al., 2013). The belt additionally contains tonalitic-granodioritic schists/gneisses, greenschist- to granulite-facies metavolcanic- sedimentary sequences, and weakly deformed Early Paleozoic mafic to acidic igneous rocks, collectively exhibiting characteristics of a collisional mélange zone. Currently identified HP-UHP rocks are distributed across the Yinggelisayi

https://doi.org/10.5194/egusphere-2025-4830
Preprint. Discussion started: 7 October 2025

(Zhang et al., 2005; Liu et al., 2005; Dong et al., 2021), Danshuiquan (Gai et al., 2022a,b), Yunusisayi (Ma et al., 2018, 2022), Jianggalesayi (Keqike) (Liu et al., 2007, 2018; Gai et al., 2017), and Munabulake (Cao et al., 2013) localities, demonstrating the belt's extensive regional continuity. The HP–UHP rocks preserve complex thermo-tectonic history, with protoliths dating to 950–730 Ma (Wang et al., 2013; Ma et al., 2022) that underwent peak metamorphism at 505–485 Ma (Zhang et al., 2001; Liu et al., 2012), followed by two distinct retrograde stages at 485–450 Ma and ~420 Ma (Liu et al., 2012; Cao et al., 2019; Dong et al., 2020; Gai et al., 2022a).

3. Sample location and selection

In the Jianggalesayi, Younusayi, and Yaolesayi, LGM rocks represented by Neoproterozoic granites are mainly distributed in the northern parts, while HP–UHP rocks represented by granitic gneisses are primarily found in the southern parts (Fig. 1b, c). The two rock units exhibit fault contact or unconformity contact (Fig. 1c).

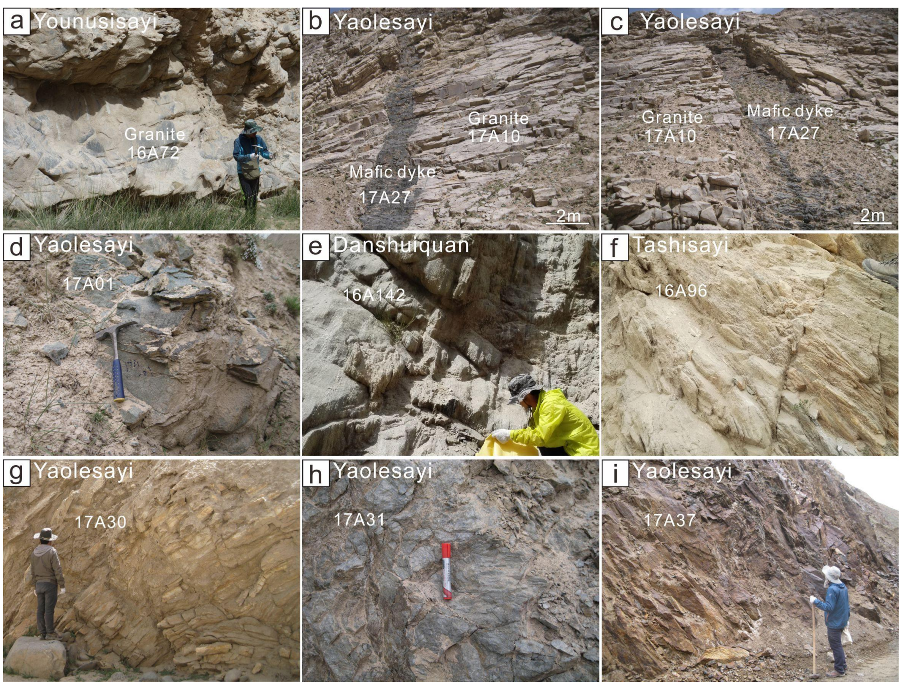

Fig.2. Field photographs taken from SAT LGM rocks. (a) Granites from Younusisayi

https://doi.org/10.5194/egusphere-2025-4830
Preprint. Discussion started: 7 October 2025

area; (b-c) Granites and mafic dykes from Yaolesayi area; (d) Amp–Pl schists from Yaolesayi area; (e) Amp–Pl schists from Danshuiquan area; (f) Bt–Pl schists from Tashisayi area; (g-h) Bt–Pl schists from Yaolesayi area; (i) Bt–Pl schists from Danshuiquan area.

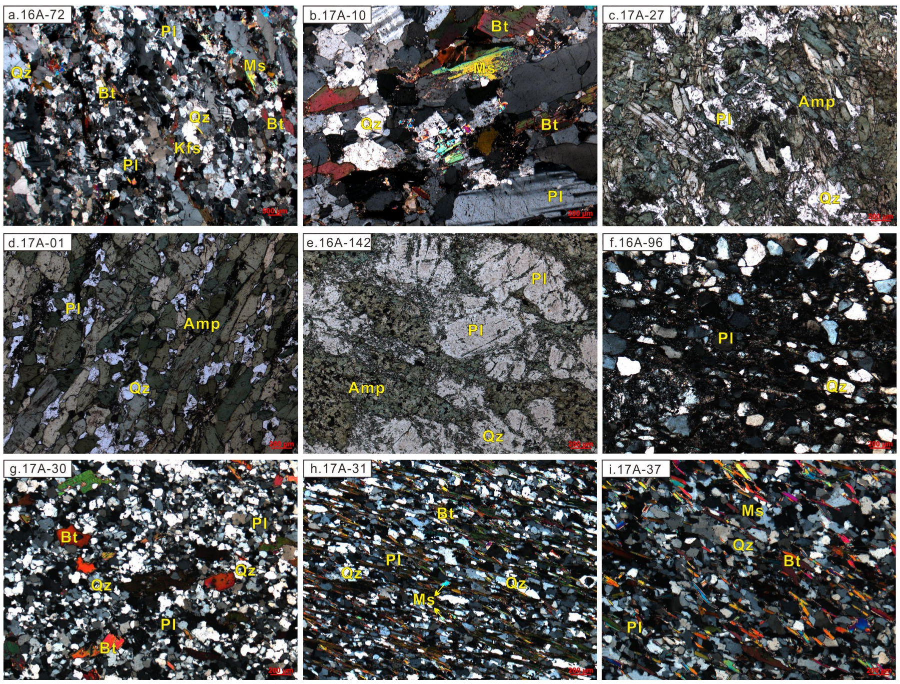

Fig.3. Microscopic photographs showing the mineralogy and texture of SAT LP–MP rocks. (a-b) Granites dominated by Qz, Pl, Bt, and a few Ms, crossed polarized light (CPL); (c) Mafic dykes dominated by Amp, Pl and a few Qz, plane polarized light (PPL); (d-e) Amp–Pl schists dominated by Amp, Pl and Qz, PPL; (f-i) Bt–Pl schists composed of Qz, Pl and minor Bt, CPL.

For the study, nine LGM rocks and three HP–UHP rocks were collected from west to east along the SAT (Fig. 1b-c). LGM rocks are widely distributed in areas such as Younusisayi, Tashisayi, Yaolesayi and Danshuiquan (Fig. 1b-c, 2, 3). Three magmatic rocks were used for formation age and protolith properties restoring. Sample 16A72 and 17A10 are taken from weakly deformed granites (Fig. 2a-b) that are dominated by quartz, feldspar, biotite, and a few muscovite (Fig. 3a-b). Sample 17A27 occurs as oriented mafic dykes intruding into granite 17A10 (Fig. 2b-c), and

https://doi.org/10.5194/egusphere-2025-4830
Preprint. Discussion started: 7 October 2025

dominated by amphibole, plagioclase and a few quartz (Fig. 3c). Six schists were used to analyze the deposition age and formation setting. Sample 17A01 and 16A142 are taken from weakly deformed Amp–Pl schists (Fig. 2d-e) that dominated by amphibole, plagioclase and quartz (Fig. 3d-e). Sample 16A96, 17A30, 17A31 and 17A37 are sampled from moderately deformed Bt–Pl schists (Fig. 2f-i) that is composed of quartz, plagioclase and contains a small amount of biotite (Fig. 3f-i), whose protolith may be sandy sedimentary rock (e.g. feldspar quartz sandstone).

HP–UHP rocks including eclogite (17A91), garnet pyroxenite (16A70), and granitic gneiss (16A69) from Younusisayi area (Fig. 1c) were used for protolith restoring. The eclogite and garnet pyroxenite occur as foliation-parallel lenses within granitic gneiss. The eclogites preserve peak mineral assemblages of Grt + Omp + Ph + Rt + Qz, recording peak *P*–*T* conditions of $P > 24.2$ kbar and $T = 710–1000$ °C (Ma et al., 2022); garnet pyroxenites contain Grt + Omp + Ms + Rt + Qz of >23.2 kbar/775–965 °C (Ma et al., 2022); granitic gneisses retain Grt + Ky + Per + Rt + Qz of 23.2–25.3 kbar/970–1010 °C (Ma et al., 2018).

Mineral abbreviations here are after Whitney and Evans (2010).

4. Zircon geochronology

LA-ICP-MS zircon U–Pb dating were conducted at State Key Laboratory of Continental Evolution and Early Life, Northwest University, China. Detailed analytical methods are provided in Supplement (Analytical method). The U–Pb isotopic and trace elements data are listed in Table S1-S12.

4.1. Granites

4.1.1. Younuisayi granite

Zircons from Sample 17A16 are colorless, and 75–150 μm in length with aspect ratios of 2.0–3.0 (Fig. 4a). Most zircon grains are euhedral to subhedral with a few prismatic grains (Fig. 4a). Zircons display clear grey oscillatory zoning and have high Th/U ratios (0.36–1.15), implying that they were derived from medium-acidic igneous protoliths.

https://doi.org/10.5194/egusphere-2025-4830
Preprint. Discussion started: 7 October 2025

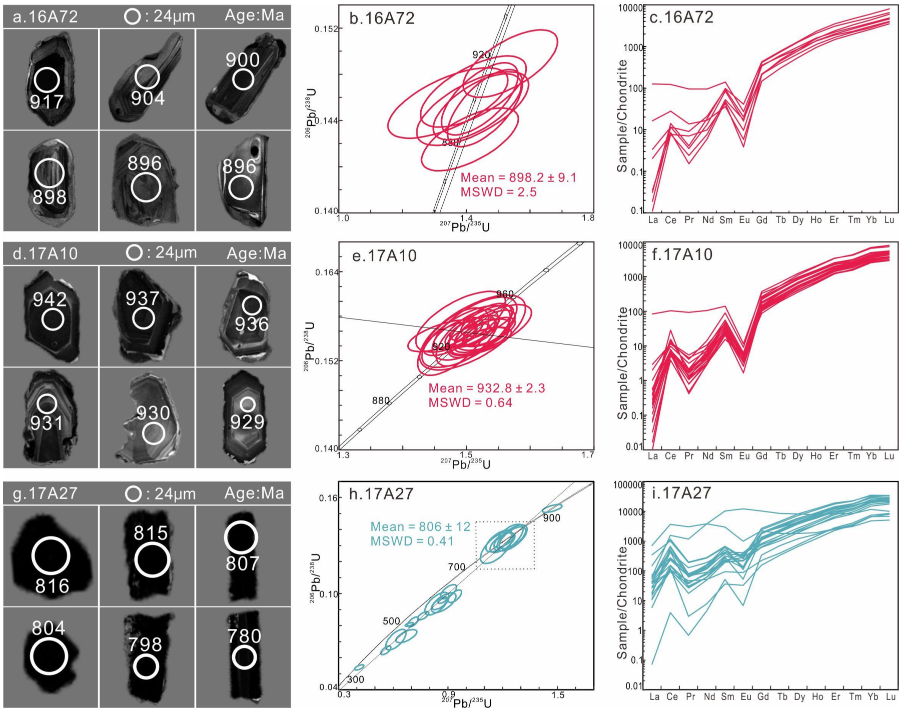

Fig.4. (a) Sample 16A72, CL images; (b) Sample 16A72, U–Pb Concordia diagram; (c) Sample 16A72, REE pattern; (d) Sample 17A10, CL images; (e) Sample 17A10, U–Pb Concordia diagram; (f) Sample 17A10, REE pattern; (g) Sample 17A27, CL images; (h) Sample 17A27, U–Pb Concordia diagram; (i) Sample 17A27, REE pattern. Normalization after Sun and McDonough, 1989.

Total 10 zircon spots were analysed and 8 concordant analyses (>95%) were accepted (Table S1). The U–Pb analytical spots plot on or close to the concordia line, forming a age groups range from 917 to 881 Ma, and yield a weighted mean age of 898.2 ± 9.1 Ma (Fig. 4b).

Zircon trace-elements data (Table S2) from 8 spots show high REE contents (Σ_{REE} = 1093.88–2555.66 ppm) and enriched HREE (Σ_{HREE} = 1058.01–2520.58 ppm), with strong negative Eu anomalies (Fig. 4c).

4.1.2 Yaolesayi granite

Zircons from Sample 17A10 are colorless, and 100–200 μm in length with aspect ratios of 1.5–3.0 (Fig. 4d). Most grains are euhedral to subhedral with a few prismatic

https://doi.org/10.5194/egusphere-2025-4830
Preprint. Discussion started: 7 October 2025

grains (Fig. 4d). Zircons display clear grey oscillatory zoning and have high Th/U ratios (0.19–0.53), implying medium-acidic igneous protoliths.

Total 21 zircon spots were analysed and 21 concordant analyses (>98%) were accepted (Table S3). The U–Pb analytical spots plot on or close to the concordia line, forming a age groups range from 942 to 927 Ma, and yield a weighted mean age of 932.8 ± 2.3 Ma (Fig. 4e).

Zircon trace-elements data (Table S4) from 23 spots show high REE contents (Σ_{REE} = 921.11–2517.63 ppm) and enriched HREE (Σ_{HREE} = 911.84–2503.36 ppm), with strong negative Eu anomalies (Fig. 4c).

4.2. Mafic dykes

Zircons from Sample 17A27 are colorless, and 50–100 μm in length with aspect ratios of 1.0–3.0 (Fig. 4g). Most grains are euhedral to subhedral with a few prismatic grains. Zircons display weak dark zoning and have high Th/U ratios (0.22–1.74).

Total 21 zircon spots were analysed and 7 concordant analyses (>98%) were accepted (Table S5). The U–Pb analytical spots plot on or close to the concordia line, forming a age groups range from 816 to 780 Ma, and yield a weighted mean age of 806.0 ± 12.0 Ma (Fig. 4h). 1 spot yield a concordant age of 918.7 ± 5.6 Ma, but its distinct oscillatory zoning suggests that the zircon may be derived from captured surrounding rock. 13 spots yield ages ranging in 621–338 Ma, all plotting on the discordia line with low concordance, likely reflecting Pb lossing.

Zircon trace-elements data (Table S6) from 7 spots show high REE contents (Σ_{REE} = 2500.71–14123.75 ppm) and enriched HREE (Σ_{HREE} = 2380.17–13787.07 ppm), with moderate negative Eu anomalies (Fig. 4i).

4.3. Schists

Detrital zircons from the studied samples are colorless to light yellow, and 50–150 μm in length with aspect ratios of 1.0–2.0 (Fig. 5a-g). Most zircon grains are rounded or ellipsoidal and generally less than 150 μm in length, indicating that they have experienced long-distance transportation and abrasion; a few grains are euhedral to subhedral with a few prismatic grains. Most zircons underwent magmatic crystals or metamorphic growth as single grain, a few zircons display clear oscillatory zoning

https://doi.org/10.5194/egusphere-2025-4830
Preprint. Discussion started: 7 October 2025

core and weak light rim.

Six schists from the Altyn Complex showed comparable detrital zircon age populations and similar Late Mesoproterozoic – Early Neoproterozoic maximum depositional ages.

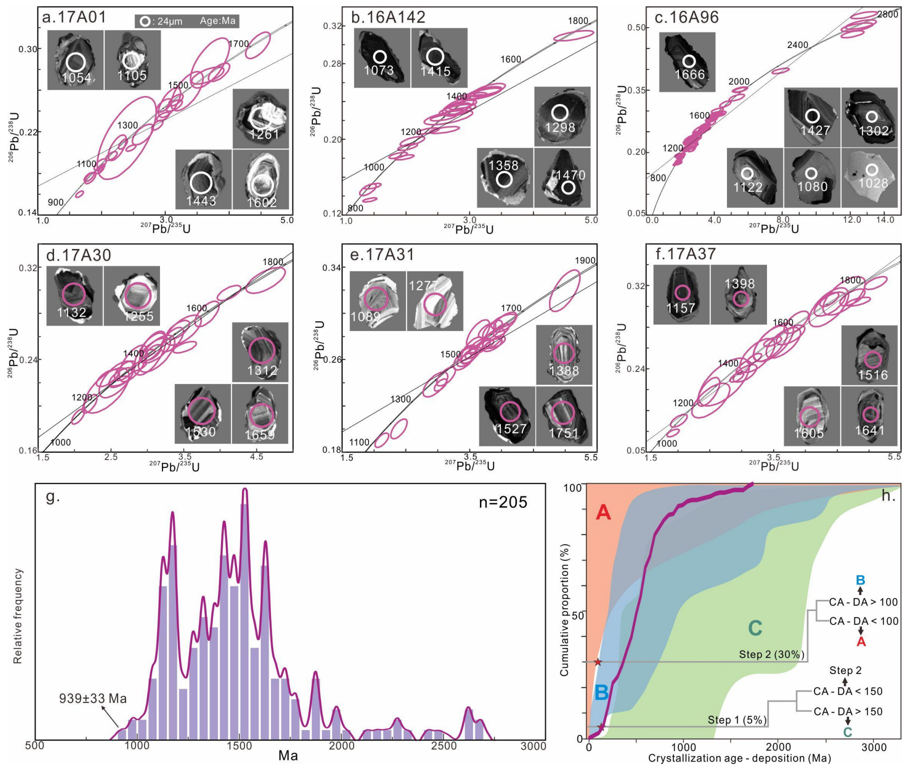

Fig.5. (a-f) Zircon U–Pb Concordia diagrams of detrital zircons from SAT schists. (g) Detrital zircon age spectra. Sources of data are available from sample 17A01, 16A142, 16A96, 17A30, 17A31 and 17A37. (h) Cumulative probability plot of detrital zircon age populations from SAT schists (after Cawood et al., 2012). A: convergent basins, B: collisional basins, C: extensional basins.

Total 205 concordant (2 points >85%, 12 points >90%, 191 points >95%) detrital zircons (zircon core of sample 17A01, 16A142, 16A96, 17A30, 17A31 and 17A37) were accepted for U–Pb dating (Table S7-S12). They exhibit a wide $^{207}Pb/^{206}Pb$ (>1.0 Ga) age range from 2658 Ma to 939 Ma (Fig. 5a-f), and with most ages being Mesoproterozoic. There is an almost continuous range in most samples from 1800 to

https://doi.org/10.5194/egusphere-2025-4830
Preprint. Discussion started: 7 October 2025

1000 Ma, with two prominent Mesoproterzoic age peaks of 1650–1400 Ma and 1200–1100 Ma on the probability density distribution plots (Fig. 5g). Small subpopulations include minor components of Neoarchean and Paleoproterozoic grains. Calculation of the youngest zircon component in each sample yielded weighted mean ages of 1055 ± 42 Ma (n = 2, MSWD = 0.078) for sample 17A01, 939 ± 33 Ma (n = 1) for sample 16A142, 995 ± 36 Ma (n = 3, MSWD = 0.28) for sample 16A96, 1139 ± 13 Ma (n = 1) for sample 17A30, 1148 ± 53 Ma (n = 2, MSWD = 0.59) for sample 17A31, 1217 ± 33 Ma (n = 1) for sample 17A37, respectively, constraining the maximum depositional ages of ca. 1150–940 Ma.

5. Whole–rock geochemistry

Whole-rock major and trace element analyses were performed at Wuhan SampleSolution Analytical Technology Co., Ltd. Detailed analytical methods are provided in Appendix *A*. The geochemical compositions of granitic and mafic rocks are listed in Table S13-S14.

5.1 Younuisayi granite

Granites (16A-72) contain high SiO_2 (71.75–72.22 wt.%), Al_2O_3 (14.35–14.56 wt %) and Na_2O+K_2O (8.60–8.82 wt %) contents, exhibiting FeO^T/MgO of 2.44–3.23, Al_2O_3/TiO_2 of 58.24–75.53, CaO/Na_2O of 0.36–0.48, K_2O/Na_2O of 1.67–1.89. Samples are classified as granite on the total alkali–silica classification diagram (Fig. 6a), exhibiting weak peraluminous on the A/CNK–A/NK diagram (Fig. 6b), alkaline affinity on the AR–SiO_2 diagram (Fig. 6c) and shoshonite affinity on the K_2O–SiO_2 diagram (Fig. 6d). Samples exhibit Σ_{REE} values of 154.23–211.54 ppm with weak negative Eu anomalies (δ_{Eu} = 0.26–0.35), light rare earth element (LREE) enrichment and distinct heavy rare earth element (HREE) depletion ($\Sigma_{LREE}/\Sigma_{HREE}$ = 34.22–35.97; $(La/Yb)_N$ = 65.74–103.12) (Fig. 7a). Samples are enriched in large ion lithophile element (LILE) and depleted in high field-strength elements (HFSE) with distinct Nb-Ta-Ti negative anomalies (Fig. 7b), while showing Th/U ratios of 8.19–11.24 and Zr/Hf ratios of 37.09–38.32.

https://doi.org/10.5194/egusphere-2025-4830
Preprint. Discussion started: 7 October 2025

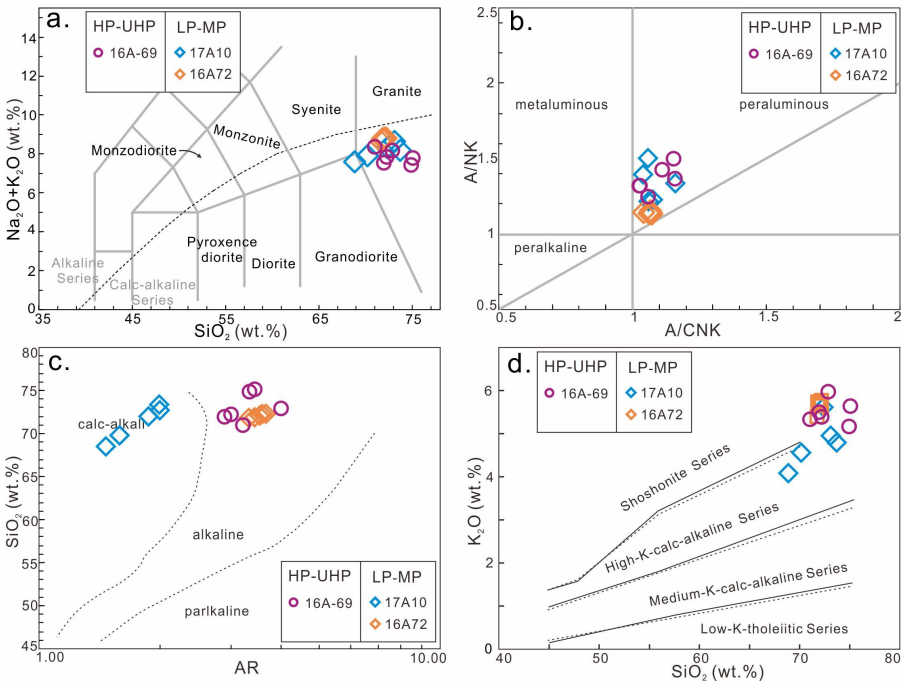

Fig.6. Geochemical characterization of granitic rocks from SAT. (a) SiO_2-(Na_2O+K_2O) diagram (Middlemost, 1994); (b) A/NK-A/CNK diagram (Maniar and Piccoli, 1989); (e) SiO_2-AR diagram (Wright, 1969); (f) K_2O-SiO_2 diagram (Rickwood, 1989).

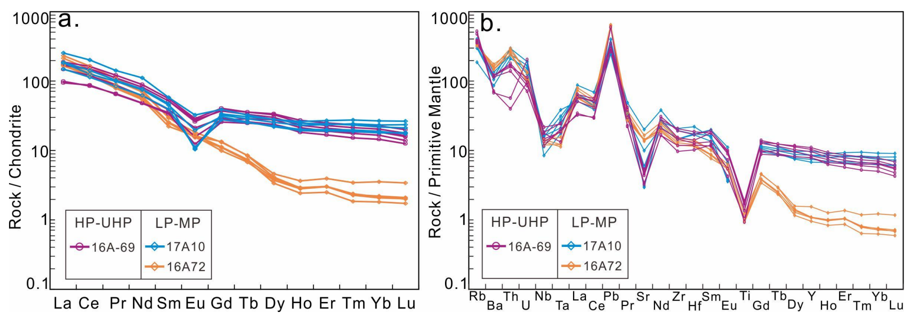

Fig.7. (a) Chondrite–normalized REE patterns for granitic rocks from SAT; (b) Primitive–mantle–normalized trace element patterns for granitic rocks from SAT.

5.2 Yaolesayi granite

Granites (17A-10) contains high SiO_2 (68.85–73.71 wt.%), Al_2O_3 (13.37–15.29 wt %) and Na_2O+K_2O (7.58–8.62 wt %) contents, exhibiting FeO^T/MgO of 4.09–15.8, Al_2O_3/TiO_2 of 37.29–102.85, CaO/Na_2O of 0.27–69, K_2O/Na_2O of 1.39–2.16. Samples are classified as granite (Fig. 6a), exhibiting weak peraluminous (Fig. 6b),

https://doi.org/10.5194/egusphere-2025-4830
Preprint. Discussion started: 7 October 2025

calc-alkali (Fig. 6c) and shoshovite affinity (Fig. 6d). Samples exhibit Σ_{REE} values of 169.68–285.60 ppm with moderate negative Eu anomalies (δ_{Eu} = 0.42–0.68), LREE enrichment and HREE depletion ($\Sigma_{LREE}/\Sigma_{HREE}$ = 6.83–9.74; $(La/Yb)_N$ = 7.05–11.71) (Fig. 7a). Samples exhibit LILEs enrichment and HFSEs depletion with distinct Nb-Ta-Ti lossing (Fig. 7b), while showing Th/U ratios of 5.57–9.14 and Zr/Hf ratios of 29.47–40.87.

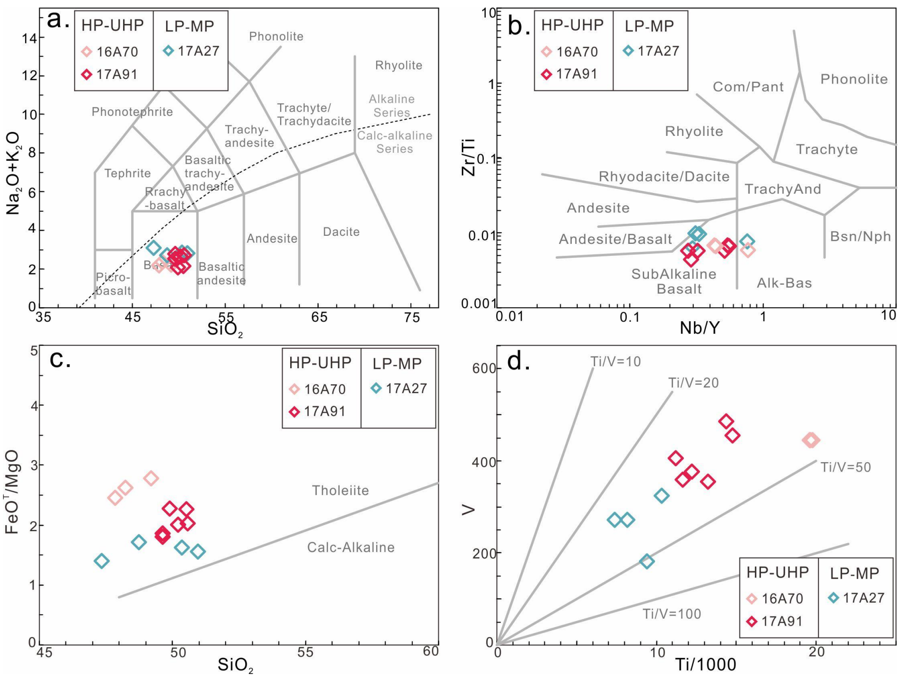

Fig.8. Major element diagrams for mafic rocks from SAT. (a) SiO_2-(Na_2O+K_2O) diagram (Maitre et al., 1989); (b) Nb/Y-Zr/Ti diagram (Winchester and Floyd, 1976); (c) SiO_2-FeO^T/MgO diagram (Miyashiro & Shido, 1975); (d) Ti/1000-V diagram (Shervais, 1982).

5.3 Younuisayi granitic gneiss

Granitic gneisses (16A-69) contain high SiO_2 (71.01–75.07 wt.%), Al_2O_3 (12.31–14.21 wt %) and Na_2O+K_2O (7.44–8.37 wt %) contents, exhibiting FeO^T/MgO of 4.36–6.75, Al_2O_3/TiO_2 of 41.79–73.17, CaO/Na_2O of 0.44–0.75, K_2O/Na_2O of 1.76–2.70. Their protolith are classified as granite (Fig. 6a), exhibiting weak peraluminous (Fig. 6b), alkaline (Fig. 6c) and shoshonite affinity (Fig. 6d).

https://doi.org/10.5194/egusphere-2025-4830
Preprint. Discussion started: 7 October 2025

Samples exhibit Σ_{REE} values of 131.15–234.34 ppm with moderate negative Eu anomalies (δ_{Eu} = 0.42–0.63), LREE enrichment and HREE depletion ($\Sigma_{LREE}/\Sigma_{HREE}$ = 5.07–7.67; $(La/Yb)_N$ = 4.82–9.58) (Fig. 7a). Samples exhibit LILEs enrichment and HFSEs depletion with distinct Nb-Ta-Ti negative anomalies (Fig. 7b), while showing Th/U ratios of 1.13–7.96 and Zr/Hf ratios of 34.60–41.84.

5.4 Yaolesayi mafic dyke

Mafic dykes (17A27) contain 47.33–50.96 wt.% SiO_2, 13.67–14.28 wt % Al_2O_3, 10.43–12.08 wt % TFeO, 6.59–8.64 wt % MgO, 7.58–10.72 wt % CaO, 1.23–1.72 wt % TiO_2, 2.72–3.11 wt % Na_2O+K_2O. They are classified as subalkaline basalt (Fig. 8a-b) of tholeiite affinity (Fig. 8c), with Ti/V ratio of 27–52 (Fig. 8d). Samples exhibit Σ_{REE} values of 68.89–97.86 ppm with slightly LREE enrichment, HREE depletion ($\Sigma_{LREE}/\Sigma_{HREE}$ =3.10–5.33; $(La/Yb)_N$ = 2.54–6.42), and weak negative Eu anomalies (δ_{Eu} = 0.28–0.33) (Fig. 10a), while showing none HFSE fractionation.

5.5 Younuisayi eclogite

Eclogites (17A91) contains 49.63–50.56 wt.% SiO_2, 12.14–14.36 wt % Al_2O_3, 12.05–14.59 wt % TFeO, 6.10–6.82 wt % MgO, 10.23–10.78 wt % CaO, 1.73–2.21 wt % TiO_2, 2.10–2.78 wt % Na_2O+K_2O. Their protolith are classified as subalkaline basalt (Fig. 8a-b) of tholeiite affinity (Fig. 8c), with Ti/V ratio of 27–38 (Fig. 8d). Samples exhibit Σ_{REE} values of 56.42–101.16 ppm with LREE enrichment or slight depletion and HREE depletion ($\Sigma_{LREE}/\Sigma_{HREE}$ = 2.06–4.36; $(La/Yb)_N$ = 1.30–4.15), and weak negative Eu anomalies (δ_{Eu} = 0.42–0.68) (Fig. 9a), while showing none HFSE fractionation and Nb–Ta negative anomalies (Fig. 9b).

5.6 Younuisayi garnet pyroxenite

Garnet pyroxenite (16A70) contains 47.85–49.20 wt.% SiO_2, 12.39–12.89 wt % Al_2O_3, 15.06–15.67 wt % TFeO, 5.44–6.38 wt % MgO, 9.93–10.14 wt % CaO, 3.27–3.30 wt % TiO_2, 2.21–2.36 wt % Na_2O+K_2O. Their protolith are classified as subalkaline basalt (Fig. 8a-b) of tholeiite affinity (Fig. 8c), with Ti/V ratio of 44–45 (Fig. 8d). Samples exhibit Σ_{REE} values of 113.83–127.93 ppm with slightly LREE enrichment, HREE depletion ($\Sigma_{LREE}/\Sigma_{HREE}$ = 3.31–3.80; $(La/Yb)_N$ = 3.13–3.72), and weak negative Eu anomalies (δ_{Eu} = 0.30–0.32) (Fig. 9a), while showing none HFSE

https://doi.org/10.5194/egusphere-2025-4830
Preprint. Discussion started: 7 October 2025

fractionation and Nb–Ta negative anomalies (Fig. 9b).

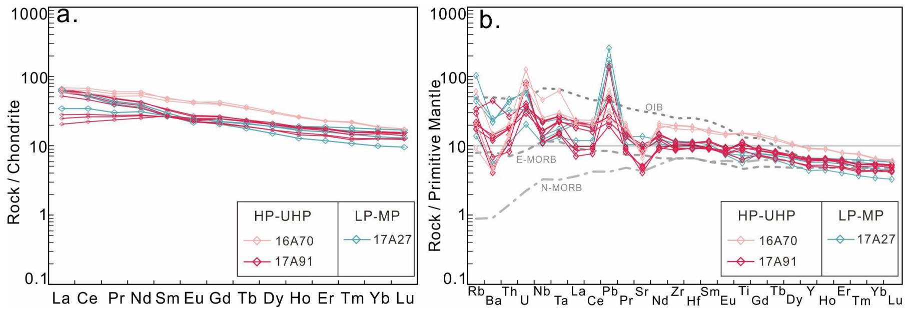

Fig.9. (a) Chondrite–normalized REE patterns for mafic rocks from SAT; (b) Primitive mantle–normalized trace element patterns for mafic rocks from SAT.

6. Discussion

6.1 Comparison of protoliths between Precambrian supracrustal rocks and HP–UHP rocks

6.1.1 Granitic rocks

Granites (LGM) and granitic gneisses (HP–UHP) in this study exhibit high-silicon, low-magnesium, (calc-)alkaline, weakly peraluminous to peraluminous characteristics, with Fe-number (FeO/FeO+MgO) of 0.67–0.93 and MALI (K_2O+Na_2O-CaO) of 5.22–7.69, FeO^T/MgO ratios of 2.44–15.84, Al_2O_3/TiO_2 ratios of 41.79–102.85, CaO/Na_2O ratios of 0.27–0.75, and K_2O/Na_2O ratios of 1.23–2.70, consistent with the geochemical features of S-type granites (SiO_2 < 74 wt.%, Al_2O_3/TiO_2 < 100, CaO/Na_2O > 0.3, K_2O/Na_2O > 1) derived from partial melting of sedimentary crustal rocks (Barbarin et al. 1999; Forst et al., 2001). The aluminous felsic magmas generated by water-saturated melting of pelitic source rocks exhibit high Sr/Ba ratios (0.08–1.6) and positive Eu anomalies; those derived from clay-rich, plagioclase-poor pelitic sources have low CaO/Na_2O (<0.3), while melts from plagioclase-rich, clay-poor psammitic sources show higher CaO/Na_2O ratios (>0.3) (Harris and Inger, 1992; Sylvester, 1998). Granites and granitic gneisses exhibit inferior Sr/Ba (0.08–0.70, except for a value of 1.83) and high CaO/Na_2O (0.27–0.75) ratio, plotting within the field of greywackes source (Fig. 10a), and further clustering

https://doi.org/10.5194/egusphere-2025-4830
Preprint. Discussion started: 7 October 2025

predominantly in the greywackes to calculated psammite-derived melt source (Fig. 10b). These characteristics suggest the common source of sandy rocks deposited by continental crust.

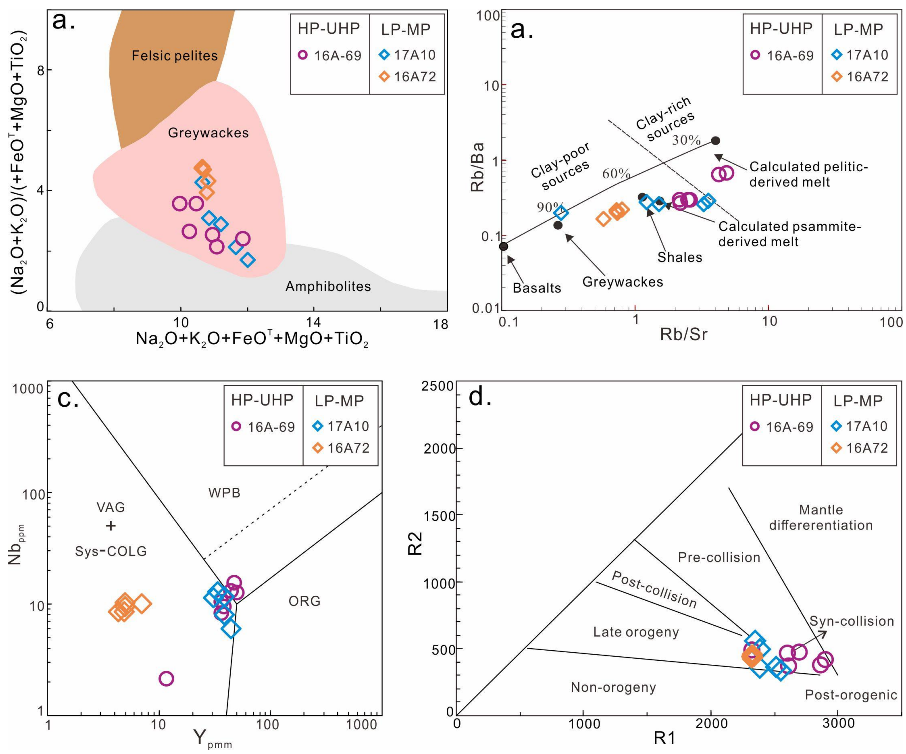

Fig.10. Source and tectonic setting discriminant diagrams for granitic rocks from SAT. (a) (Na_2O + K_2O + FeO^T + MgO + TiO_2) vs. (Na_2O + K_2O)/(FeO^T + MgO + TiO_2) diagram (Douce, 1999); (b) Rb/Sr vs Rb/Ba diagram (Sylvester et al., 1998); (c) Y-Nb diagram (Pearce et al., 1984); (d) R_1-R_2 diagram (Batchelor and Bowden, 1985).

Melting pressures are constrained by residual phases, with garnet indicating HP (>10 kbar) conditions and plagioclase signifying low-pressure origins (Defant and Drummond, 1990). Trace elements constrain pressures: high Sr (>300 ppm) without Eu anomaly indicates plagioclase-absent residues, while low Y (<15 ppm), high Sr/Y (>20), low Yb (<1.9 ppm), and high La/Yb (>20) suggest garnet retention (Zhang Q, 2006, 2010; Castillo et al., 2006). Granites (17A10) and granitic gneisses (16A69) exhibit moderate Sr (62.41–430.98 ppm), negative Eu anomalies (δ_{Eu} = 0.09–0.36),

https://doi.org/10.5194/egusphere-2025-4830
Preprint. Discussion started: 7 October 2025

high Y (11.56–49.98 ppm) and Yb (1.20–4.53 ppm), low Sr/Y (1.40–10.87, except for a value of 37.27) and La/Yb (6.81–16.32), indicating plagioclase-bearing but garnet-absent residues and LP formation conditions. While granites (16A72) exhibit moderate Sr (288.03–350.25 ppm), negative Eu anomalies (δ_{Eu} = 0.26–0.35), low Y (4.34–7.02 ppm) and Yb (0.31–0.60 ppm), high Sr/Y (49.86–70.26) and La/Yb (91.65–143.76), indicating garnet-bearing residues and HP formation conditions.

Their tectonic affinities are further constrained by Nb-Y (Fig. 10c) and R_1-R_2 (Fig. 10d) diagrams, which consistently classify them as syn-collisional to orogenic granites. The granites emplaced at 898.2 ± 9.1 Ma (Fig. 4b) and 932.8 ± 2.3 Ma (Fig. 4e), and the protolith of granitic gneiss formed at 900.2 ± 4.1 Ma (Ma et al., 2018). Their geochemical signatures demonstrate typical crustal melting characteristics and syncollisional granite affinities, which are consistent with contemporaneous granitic gneisses (HP–UHP) from Danshuiquan and Bashiwake (Liu et al., 2004; Zhu et al., 2014; Gai et al., 2022b). Meanwhile, Neoproterozoic (965–890 Ma) crust-derived S-type granites are extensively developed in the Yaganbuyang, Huanxingshan, Gailike, Kuoshi, and Kekesayi areas of the CAB and SAT (Yu et al., 2013; Wang et al., 2013). These granites are also weakly peraluminous or peraluminous, enriched in LILEs and LREEs, and depleted in some HFSEs and HREE, exhibiting typical continental crust features without clear Early Paleozoic metamorphic evidence (Wan et al., 2001; Peng et al., 2019).

Combining this study with previous data, the granites (LGM) and granitic gneisses (HP–UHP) from CAB and SAT share similar protoliths but exhibit significant difference in mineral assemblages and metamorphic-deformation histories, suggesting they likely formed in the same tectonic setting, with the former (granites) not involved in the SAT Early Paleozoic continental deep subduction.

6.1.2 Mafic rocks

Mafic dykes (LGM), eclogites and garnet pyroxenites (HP–UHP) exhibit slightly lower SiO_2 (47.33–50.96 wt.%), MgO (5.44–8.64 wt.%), Cr (59–277), Ni (51–114 ppm), Sc (21–41 ppm), Co (64–242 ppm), and $Mg^{\#}$ (43–60) than primary magma

https://doi.org/10.5194/egusphere-2025-4830
Preprint. Discussion started: 7 October 2025

(Frey and Prinz, 1978), reflecting that their protolith underwent weak fractional crystallization from primary magma with mantle source. They exhibit negligible anomalies in Nb, Ta, and Ti (Fig. 9b), coupled with low $(Th/Nb)_{PM}$ ratios (<1.52, except for two values of 3.35 and 3.48), and high Nb/La ratios (0.61–2.13), reflecting very weak crustal contamination (Nb/Ta/Ti depletion, Nb/La < 1, $(Th/Nb)_{PM}$ > 2, crustal input) (Rudnick and Gao, 2003; Ernst, 2014; Kieffer et al., 2004). In Nb/Yb-Th/Yb and $(Th/Nb)_{PM}$-$(La/Nb)_{PM}$ diagram, the mafic dykes (two data) fall in active continetal margin (Fig. 11a), and between the oceanic basalt and lower crust (Fig. 11b), which indicates that may be weakly contaminated by lower crust materials during the formation process (Frey et al., 2002; Fitton et al., 1998).

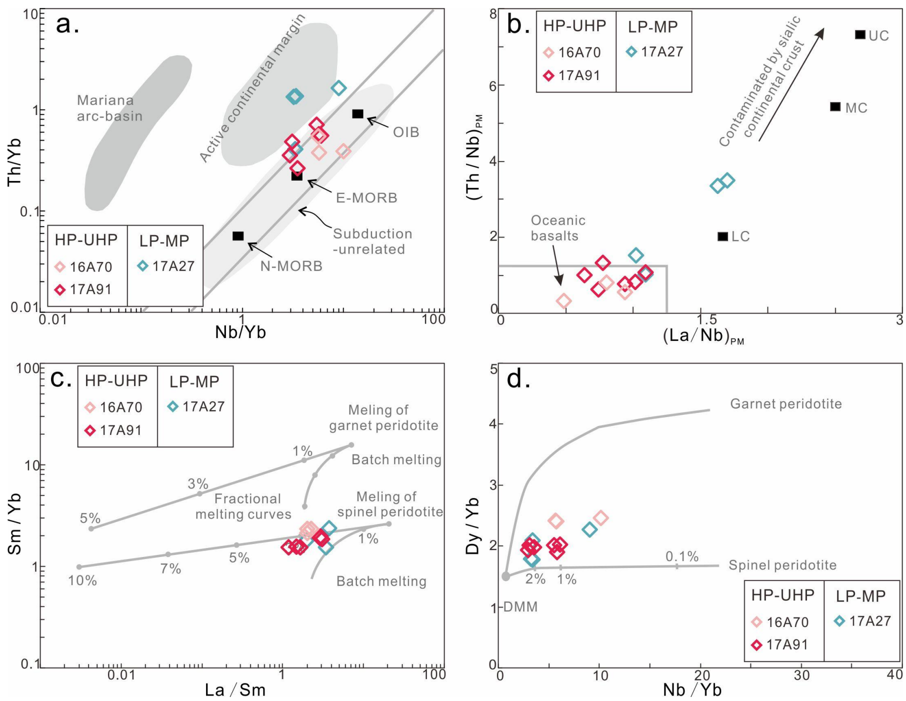

Fig.11. (a) Th/Yb-Nb/Yb diagram (Pearce, 1982, 2008); (b) Th/Nb_{PM}-La/Nb_{PM} diagram (Frey et al., 2002); (c) Th/Yb-Nb/Yb diagram (Pearce, 2008); (d) Nb/Yb-TiO_2/Yb diagram (Pearce, 2008).

Mafic dykes, eclogites and garnet pyroxenites exhibit low La/Nb (0.47–1.64) and La/Ta (6.01–21.97) ratios, effectively exclude lithospheric mantle (La/Nb > 1.5; La/Ta > 22) contributions (Fitton et al., 1988; Saunders et al., 1992). Their high TiO_2

https://doi.org/10.5194/egusphere-2025-4830
Preprint. Discussion started: 7 October 2025

(1.23–3.30 wt.%) and $Fe_2O_3^T$ (11.59–17.42 wt.%) contents along with coherent trace element trends (Fig. 9a, b), demonstrating a common asthenospheric mantle source (Falloon et al., 1988; Hirose and Kushiro, 1993). The fractionation-resistant Tb/Yb ratio reliably constrains mantle source depth, clearly distinguishing garnet- ((Tb_N/Yb_N >1.8) from spinel-facies (Tb_N/Yb_N <1.8) stability fields (Wang et al., 2002). Their low Tb_N/Yb_N (1.31–1.96) ratios indicate a spinel-bearing mantle peridotite source, further supported by their consistent placement within the spinel lherzolite melting field on both La/Sm-Sm/Yb (Fig. 11c) and Nb/Yb-Dy/Yb (Fig. 11d) diagrams.

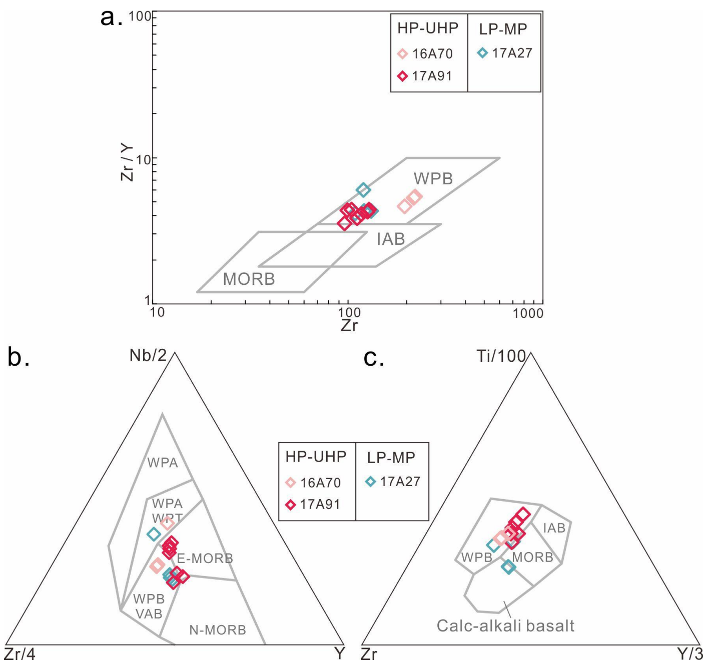

Fig.12. Trace element discrimination diagrams for tectonic setting for mafic rocks from SAT. (a) Zr-Zr/Y diagram (Pearce and Norry, 1979); (b)) Nb/2-Zr/4-Y diagram (Mullen, 1983); (c) 100Ti-Zr-3Y diagram (Meschede, 1986).

Mafic dykes, eclogites and garnet pyroxenites exhibit enriched LILEs and LREEs, flat HREEs, none HFSEs depletion, and insignificant Eu anomalies, along with typical Ta/Hf (0.19–0.23), Nb/Zr (0.07–0.09), Th/Ta (3.15–3.54), and La/Nb (1.03–1.49) ratios. They consistently plot within the within-plate basalt field across

https://doi.org/10.5194/egusphere-2025-4830
Preprint. Discussion started: 7 October 2025

multiple discrimination diagrams, including Zr-Zr/Y (Fig. 12a), Zr/4-Nb/2-Y (Fig. 12b), Zr-Ti/100-Y/3 (Fig. 12c) diagrams. The comprehensive geochemical evidence indicate the continental intraplate tectonic setting. The mafic dikes emplaced at 806 ±12 Ma (Fig. 4h), the eclogites's protolith (17A91) formed at 902.7 ± 6.4 Ma (Ma et al., 2022), garnet pyroxenites's protolith developed between 906–811 Ma (Ma et al., 2022). Thus, the formation of these mafic rocks from continental extension to rift during 903–806 Ma indicates that the Altyn region transitioned from a collision background to an extension regime since ~900 Ma. This is further corroborated by subsequently extensive rift-related magmatism, such as the 850–820 Ma A1-type granites, followed by 780–750 Ma bimodal intraplate magmatism and 620–580 Ma volcanism (Hao et al., 2020).

Consistent formation setting and similar ages demonstrate that mafic dikes and protoliths of eclogites/garnet pyroxenites represent mafic intrusions emplaced into Neoproterozoic granites (16A69, 17A10) during during Rodinia's rifting. The protoliths of eclogites/garnet pyroxenites were involved in Early Paleozoic continental deep subduction and underwent HP–UHP metamorphism, while the mafic dikes escaped subduction and retained pristine magmatic dike morphology (Fig. 2b-c).

6.1.3 Sedimentary rocks

Detrital zircons of six samples from the Altyn Complex demonstrate the dominance of Mesoproterozoic grains (ca. 1600–1000 Ma), yielding maximum depositional ages of ca. 1150–939 Ma (Fig. 5g). This indicates that the sedimentary protoliths of the Altyn Complex were deposited no earlier than 940 Ma. Early Neoproterozoic granites intruding into the Altyn Complex (meta-)sedimentary rocks were dated at 932–898 Ma. Thus, we propose that the metasedimentary rocks of the Altyn Complex were deposited during a narrow time interval between 939–932 Ma.

Detrital zircon age spectra of sedimentary basins serves as indicator of regional tectonic evolution, with distinct provenance signatures reflecting specific tectonic environments (Cawood et al., 2007, 2012; Ksienzyk and Jacobs, 2015). The sediment

https://doi.org/10.5194/egusphere-2025-4830
Preprint. Discussion started: 7 October 2025

source-to-sink processes and tectonic settings can be visualized and interpreted through crystallization versus depositional age (CA–DA) diagrams. For SAT LGM rocks, the CA–DA lines dominantly plot within the collisional basins field (B), though in areas overlapping either with convergent or extensional fields (Fig. 5h). Notably, (meta-)sedimentary rocks within Altyn Complex, unaffected by early Paleozoic HP-UHP metamorphism, displays three diagnostic features matching the Taxidaban Group: ① identical lithological associations; ② indistinguishable detrital zircon age spectra (Fig. 5g); and ③ congruent maximum depositional ages. These robust correlations indicate that they are part of the same late Mesoproterozoic to Neoproterozoic (meta-)sedimentary sequence, a conclusion also reported in Hao et al. (2023).

6.2 Genesis of LGM rocks (retrograde overprinting and non-subduction)

The formation of LGM rocks in orogens involves multiple geneses: a. HP–UHP rocks are thermally reset to LGM assemblages during exhumation; b. overriding plate dragged into shallow-depth antithetic subduction by the subducting slab (Liu et al., 2018); c. detachment and exhumation of subducted slabs at relatively shallow depths within the subduction channel (Zheng, 2012); d. tectonic mélanges scraped off and accreted onto the subduction zone during plate subduction (Zhou, 2004, 2020; Zheng et al., 2005); and e. non-subducted overlying plate (Sizova et al., 2012; Maierová., 2021; Yin et al., 2007).

The SAT LGM rocks can be classified into two types based on their genesis: retrograde overprinting and non-subduction origin.

Besides typical HP–UHP rocks (e.g., coesite eclogites; Gai et al., 2017), the SAT hosts widespread lower-grade metamorphic rocks, including pelitic/granitic gneisses, amphibolites lenses, and metamorphosed mafic interlayers (Liu et al., 2012; Wang et al., 2013). Petrological, mineralogical and thermodynamical modeling studies reveal that most of these rocks preserve mineralogical evidence of early-stage HP–UHP metamorphism, such as: ① Phengite inclusions in zircon and garnet compositional zoning in Yaganbuyang amphibolites suggest a UHP peak condition (Li et al., 2023);

https://doi.org/10.5194/egusphere-2025-4830
Preprint. Discussion started: 7 October 2025

② (401)-oriented exsolution of pigeonite from clinopyroxene in Bashiwake garnetites, with reconstructed C2/c pyroxenes, suggest the 6–7 GPa formation pressures; ③ Exsolution of spinel+kyanite from quartz in Jianggalesayi gneisses, interpreted as decompression products after Al+Fe^{3+}-bearing stishovite breakdown, implying >300 km subduction depths (Liu et al., 2007); ④ Garnet+clinopyroxene inclusions in zircon in Munabulake amphibolites (Unpublished data) suggest the eclogite-facies peak condition. These findings demonstrate that portions of the SAT LGM rocks underwent deep continental subduction, although their HP–UHP records were obliterated by subsequent retrograde metamorphic events (Fig. 13).

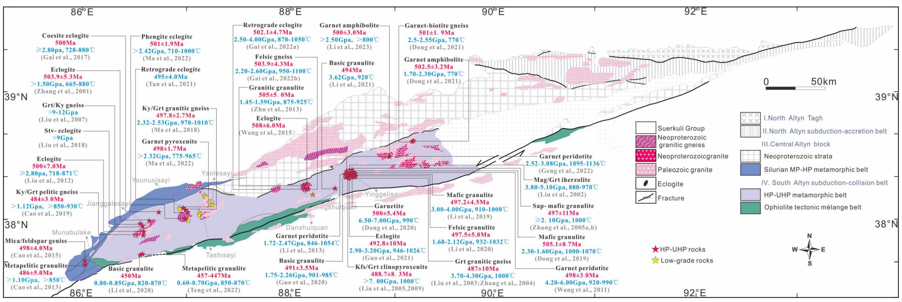

Fig.13. Summarizing of distribution locations, peak metamorphic ages, and *P*–*T* conditions of various metamorphic rocks from South Altyn.

Meanwhile, the SAT exposes a greenschist-facies metasedimentary sequence, comprising quartzite, mica schist, quartz schist, feldspathic quartz schist, and carbonate rocks, with formation ages of 1084–939 Ma (Late Mesoproterozoic to Early Neoproterozoic) and Taxidaban Group affinities (Hao et al., 2023; this study). Granites intruded into Mesoproterozoic sedimentary formation during 954–896 Ma, without apparent metamorphic/deformation modification (Peng et al., 2019 and its references). And the mafic dyke retaining original occurrence, which firstly reported in the SAT in this study. These rock assemblages show clear similarities with those of the CAB (RGXR, 1993; Hao et al., 2023), supporting their interpretation as remnants of the overlying plate unaffected by subduction.

https://doi.org/10.5194/egusphere-2025-4830
Preprint. Discussion started: 7 October 2025

6.3 Geological significance

6.3.1 Emplacement process: LGM vs. HP–UHP rocks

Preceding discussion have yielded two key findings: a. the protoliths of LGM rocks in the SAT exhibit consistency with those of HP–UHP rocks; b. the protolith composition of these metamorphic rocks shows strong affinity with the rock assemblages of the CAB. Then, how to understand the formation and differential evolution of these rocks?

Integrating the Meso-Neoproterozoic to Early Paleozoic magmatic, sedimentary, and metamorphic records of the South Altyn Tagh, the emplacement of the SAT metamorphic rocks (LGM vs. HP–UHP rocks) likely underwent the following stages (Fig. 11):

(a) > 900 Ma: widespread sedimentary cover sequences and intrusive granites were formed during Rodinia assembly. This process gave rise to formation of Meso- to Neoproterozoic metasedimentary and volcanic successions (RGXR, 1993; RGGX, 2003), granite (Gehrels et al., 2003b; Wang et al., 2013; Chen et al., 2018a, b), granodiorite, etc.

(b) 900–520 Ma: during the breakup of the supercontinent, the SAT and CAB were rifted apart into two separate units with emplacement of mafic dikes (this study), while maintaining identical lithological compositions (including granites, sedimentary cover, and intraplate basaltic-affinity mafic intrusions).

(c-d) 520–480 Ma: the SAT subducted beneath the CAB (Liu et al., 1998; Yao et al., 2021), generating SAT HP–UHP rocks (Liu et al., 2012). The Neoproterozoic granite, mafic rock and sediments in the SAT were transformed into granitic gneiss, eclogite, pelitic gneiss, etc (Fig. 13 and it's references).

(e-f) 480–420 Ma: the deeply subducted slab underwent exhumation, leading to the juxtaposition of HP–UHP rocks (SAT) with unsubducted LGM rocks (from CAB) in the current SAT terrane.

https://doi.org/10.5194/egusphere-2025-4830
Preprint. Discussion started: 7 October 2025

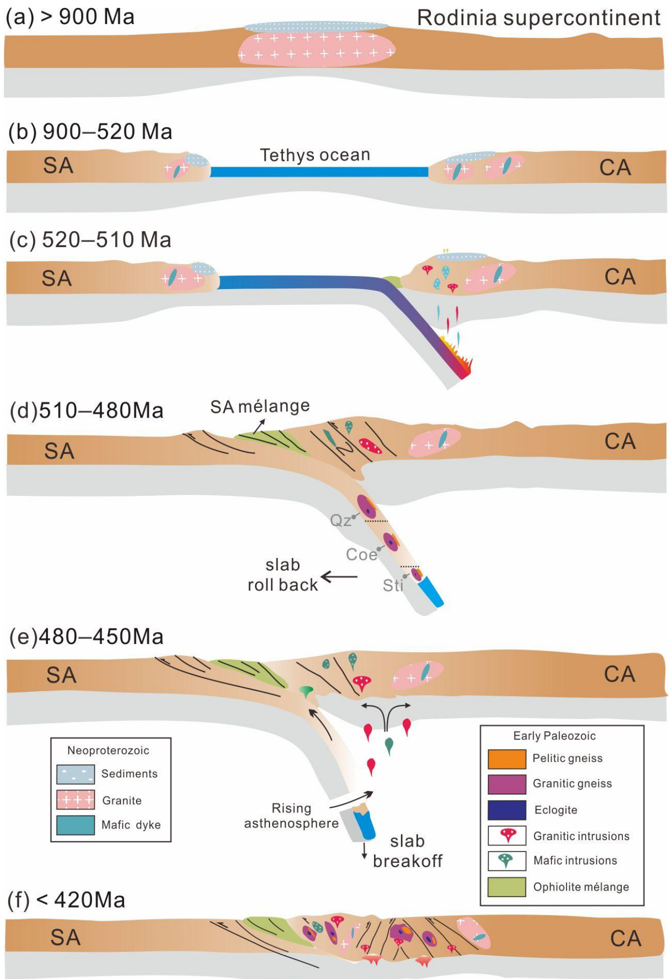

Fig.14. Schematic illustration showing the proposed multi-stage evolution of the South Altyn and the tectonic positioning process of various rocks

6.3.2 Consistent subduction, differential exhumation and modification

The rocks (e.g. eclogites, garnet pyroxenites, amphibolites, garnet peridotites, and Ky/Grt-bearing granitic/pelitic gneisses, etc.) with Early Paleozoic HP–UHP records are extensively distributed in the Munabulake, Jianggalesayi, Younussayi, Danshuiquan, Yinggelisayi, Yaganbuyang and other localities, spanning the entire SAT from west to east (Fig. 13 and it's references). These rocks established a fundamental understanding that the UHP rocks in both eastern and western SAT sections underwent widespread continental crust subduction, reaching eclogite-facies

https://doi.org/10.5194/egusphere-2025-4830
Preprint. Discussion started: 7 October 2025

or even higher-grade metamorphic conditions, consistent with overall subduction characteristics. However, the spatiotemporal relationships and metamorphic evolution of HP–UHP and LGM rocks exhibit distinct differences between the eastern and western SAT sections (Gai et al., 2022a, b).

Numerical modeling reveals two primary exhumation mechanisms for deeply subducted continental crust: a. subduction-channel exhumation (Gerya, 2002; Warren et al., 2008), characterized by "low-grade accretionary wedge → HP belt → UHP dome → HP belt → Ophiolite mélange→ low-grade accretionary wedge" spatial pattern (Beaumont et al., 2009; Li et al., 2011); and b. diapiric ascent (Hall and Kincaid, 2001; Little et al., 2011; Li, 2014), HP–UHP terranes instead form domes within the overriding plate's low-grade rocks, showing: "overriding plate → HP/UHP dome → overriding plate" (Maierová et al., 2021).

In the eastern SAT (Danshuiquan and Yinggelisayi, etc), HP–UHP rocks (granitic/pelitic gneisses, eclogites, garnet pyroxenite, etc) form oval to semi-circular landforms, in fault contact with LGM surrounding rocks (pelitic schist/gneiss, marble, and ultrabasic rocks), displaying a dome-like distribution pattern (Fig. 15a-b). HP–UHP rocks experienced eclogite-facies peak metamorphism at ~500 Ma and subsequent HP granulite facies retrogression at ~480 Ma, with near-isothermal decompression during initial exhumation accompanied by intense HP–UHT retrograde metamorphism (Dong et al., 2019; Gai et al., 2022a). Meanwhile, Gai et al. (2024) noted a significant partial melting in the felsic gneisses of the eastern SAT, which reduced viscosity and enhanced buoyancy, thereby promoting the rapid exhumation of the HP–UHP terrane. These geological observations align with the typical characteristics of diapiric exhumation (Fig. 15c) (Hacker and Gerya, 2013). Dong et al. (2021, 2025) also employed a diapiric model to explain the exhumation of the Early Paleozoic UHP terrane in the SAT.

In contrast, western sections (Jianggalesayi, Younusisayi, and Yaolesayi) show mixed HP–UHP and LGM rocks of varying scales without distinct dome structures. Notably, HP–UHP rocks from Jianggalesayi/Younusisayi and LGM rocks from Yaolesayi are suspected to form a banded/zonal distribution pattern (Fig. 1c).

https://doi.org/10.5194/egusphere-2025-4830
Preprint. Discussion started: 7 October 2025

HP–UHP rocks exhibits eclogite-facies peak metamorphism at ~500 Ma but slightly younger granulite-facies retrogression during 460–450 Ma, with cooling-decompression retrograde *P–T–t* paths (Liu et al., 2012; Ma et al., 2022).

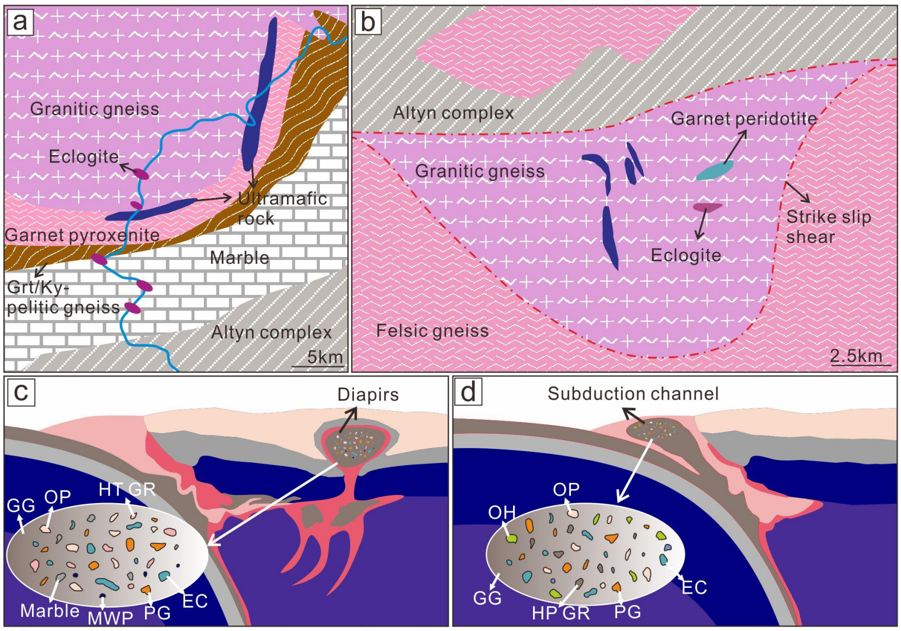

GG-granitic gneiss; EC-eclogite; PG-pelitic gneiss; GR-granilite; OP-overlying plate; MWP-mantle wedge peridotite: OH-ophiolite

Fig.15. (a-b) Simplified geological map shows the contact relationships of different rocks in Danshuiquan and Bashiwake. (c-d) Proposed mechanism for the formation of HP–UHP rocks, involving the growth of a trans-lithospheric diapir and exhumation along the subduction channel (modified from Maierová et al., 2021).

Based on the spatial distribution characteristics of the HP–UHP metamorphic terrain and combined with studies of metamorphism, we further confirm that the eastern and western sections of the SAT have undergone different exhumation processes (Gai et al., 2022a). The HP–UHP rocks in Yunusisayi/Jianggalesayi show subduction-channel exhumation (Fig. 15d), contrasting with Yaolesayi LGM rocks (may represent the overlying plate; sample 17A- 01, 09,10, 27, 30, 31, 37). The Danshuiquan/Yinggelisai HP–UHP granitic gneisses with mafic units form diapiric cores, with the surrounding schists/gneisses (sample 16A142) representing the upper plate.

https://doi.org/10.5194/egusphere-2025-4830
Preprint. Discussion started: 7 October 2025

In addition, differential retrograde metamorphic overprinting is also responsible for the significant variations in preserved mineral assemblages (HP–UHP or LGM) among SAT different metamorphic rocks. It is mainly manifested in the control of two factors: a. most HP–UHP mineralogical records tend to be erased by the intense deformation at crustal depths (~30 km), with weakly deformed felsic gneisses preserving complete *P*–*T* paths (peak, 2.2–2.6 GPa, 950–1100 °C), whereas strongly deformed gneisses retain only retrograde (0.87–1.1 GPa, 750–770 °C) assemblages (Gai et al., 2022b); b. partial melting destroys early HP–UHP minerals while enhancing the rheology of subducted slabs, facilitating the exhumation of HP–UHP rocks (Gai et al., 2024).

7. Conclusion

(1) The SAT extensively develops LGM rocks, lacking obvious Cambrian metamorphic overprinting. They shares similar protolith ages and characteristics with SAT HP–UHP rocks, suggesting a common stratigraphic origin but significantly different pre-subduction tectonic relationships. This contrast indicates that these pre-cambrian crust rocks may represent the unsubducted overlying plate (i.e., the CAB).

(2) HP–UHP rocks are widely developed from east to west, indicating a consistent continental subduction.

(3) The modern spatiotemporal positioning status of SAT HP–UHP rocks and LGM rocks is formed due to the differential exhumation and modification of the deep subducted continental crust.

Data availability

All data generated or analysed during this study are included in this published article.

Author contributions

Tuo Ma completed the experiment, collected and processed the data and wrote the manuscript. YongSheng Gai and Xiaoying Liao participated in the experimental analysis and discussion.

Competing interests

The contact author has declared that none of the authors has any competing interests.

Disclaimer

Publisher's note: Copernicus Publications remains neutral with regard to jurisdictional claims made in the text, published maps, institutional affiliations, or any other geographical representation in this paper. While Copernicus Publications makes every effort to include appropriate place names, the final responsibility lies with the authors.

Financial support

This work was supported by National Natural Science Foundation of China (grant no. 42030307, 42302056, 41972054) and MOST Special Fund from the State Key Laboratory of Continental Evolution and Early Life.

References

Andersen, T. B., Jamtveit, B., Dewey, J. F., and Swensson, E.: Subduction and eduction of continental crust: major mechanisms during continent–continent collision and orogenic extensional collapse, a model based on the south Norwegian Caledonides, *Terra Nova*, 3, 303–310, 1991.

Barbarin, B.: A review of the relationships between granitoid types, their origins and their geodynamic environments, *Lithos*, 46, 605–626, 1999.

Batchelor, R. A. and Bowden, P.: Petrogenetic interpretation of granitoid rock series using multicationic parameters, *Chemical Geology*, 48, 43–55, 1985.

Beaumont, C., Jamieson, R. A., Butler, J. P., and Warren, C. J.: Crustal structure: A key constraint on the mechanism of ultra–high–pressure rock exhumation, *Earth and Planetary Science Letters*, 287, 116–129, 2009.

Brueckner, H. K.: The great eclogite debate of the Western Gneiss Region, Norwegian Caledonides: The in situ crustal v. exotic mantle origin controversy, *Journal of Metamorphic Geology*, 36, 517–527, 2018.

Cao, Y., Du, J. X., Park, M., Jung, S., Park, Y., Kim, D., Choi, S., Jung, H., and Austrheim, H.: Metastability and nondislocation–based deformation mechanisms of the Flem eclogite in the Western Gneiss Region, Norway, *Journal of Geophysical Research: Solid Earth*, 125, e2020JB019375, https://doi.org/10.1029/2020JB019375, 2020.

Cao, Y. T., Liu, L., Wang, C., Kang, L., and Liao, X. Y.: Timing and nature of the partial melting processes during the exhumation of the garnet–bearing biotite gneiss in the southern Altyn Tagh HP/UHP belt, Western China, *Journal of Asian Earth Sciences*, 170, 274–293, 2019.

https://doi.org/10.5194/egusphere-2025-4830
Preprint. Discussion started: 7 October 2025

Cao, Y. T., Liu, L., Wang, C., Yang, W. Q., and Ying, L. X.: Determination and implication of the HP pelitic granulite from the Munabulake area in the South Altyn Tagh, *Acta Petrologica Sinica*, 29, 1727–1739, 2013.

Castillo, P. R.: An overview of adakite petrogenesis, *Chinese Science Bulletin*, 51, 257–268, 2006.

Cawood, P. A., Hawkesworth, C. J., and Dhuime, B.: Detrital zircon record and tectonic setting, *Geology*, 40, 875–878, 2012.

Cawood, P. A., Nemchin, A. A., Strachan, R., Prave, T., and Krabbendam, M.: Sedimentary basin and detrital zircon record along East Laurentia and Baltica during assembly and breakup of Rodinia, *Journal of the Geological Society*, 164, 257–275, 2007.

Chen, H. J., Wang, N., Wu, C. L., Lei, M., Zheng, K., Zhang, X., and Gao, D.: Geochemistry, Zircon U-Pb dating and Hf isotopic characteristics of Neoproterozoic granitoids in the Yaganbuyang area, Altyn Tagh, NW China, *Acta Geologica Sinica (English Edition)*, 92, 1366–1383, 2018b.

Chen, H. J., Wu, C. L., Lei, M., Guo, W. F., Zhang, X., Zheng, K., Gao, D., and Wu, D.: Petrogenesis and implications for Neoproterozoic granites in Kekesayi Area, South Altyn continent, *Earth Science-Journal of China University of Geosciences*, 43, 1278–1292, 2018a.

Chopin, C.: Ultrahigh–pressure metamorphism: tracing continental crust into the mantle, *Earth and Planetary Science Letters*, 212, 1–14, 2003.

Defant, M. J. and Drummond, M. S.: Derivation of some modern arc magmas by melting of young subducted lithosphere, *Nature*, 347, 662–665, 1990.

Dong, J. and Wei, C.: Multi-episode metamorphism and magmatism in the paleozoic altyn orogen, west china: implications for the tectonic evolution of the proto-tethys ocean, *Earth-Science Reviews*, 262, 105067, https://doi.org/10.1016/j.earscirev.2024.105067, 2025.

Dong, J., Wei, C., and Zhang, J.: Ultra high temperature metamorphism of mafic granulites from South Altyn Orogen, West China: A result from the rapid exhumation of deeply subducted continental crust, *Journal of Metamorphic Geology*, 37, 315–338, https://doi.org/10.1111/jmg.12464, 2019.

Dong, J. and Wei, C. J.: Multi–stage metamorphism of the South Altyn ultrahigh–pressure metamorphic belt, West China: insights into tectonic evolution from continental subduction to arc–backarc extension, *Journal of Petrology*, 62, egab082, https://doi.org/10.1093/petrology/egab082, 2021.

Dong, J., Wei, C. J., Chen, J., et al.: P–T–t path of garnetites in South Altyn Tagh, West China: a complete record of the ultradeep subduction and exhumation of continental crust, *Journal of Geophysical Research: Solid Earth*, 125, e2019JB018881, https://doi.org/10.1029/2019JB018881, 2020.

Douce, A. E. P.: What do experiments tell us about the relative contributions of crust and mantle to the origin of granitic magmas?, *Geological Society, London, Special Publications*, 168, 55–75, 1999.

Ernst, R. E.: Large Igneous Provinces, Cambridge University Press, Cambridge, pp. 1–653, 2014.

Ernst, W. G.: Preservation/exhumation of ultrahigh–pressure subduction complexes, *Lithos*, 92, 321–335, 2006.

Falloon, T. J., Green, D. H., Hatton, C. J., et al.: Anhydrous partial melting of a fertile and depleted peridotite from 2 to 30 kb and application to basalt petrogenesis, *Journal of Petrology*, 29, 1257–1288, 1988.

Fitton, J. G., James, D., Kempton, P. D., et al.: The Role of Lithospheric Mantle in the Generation of Late Cenozoic Basic Magmas in the Western United States, *Journal of Petrology*, 29, 331–349, 1988.

Frey, F. A. and Prinz, M.: Ultramafic inclusions from San Carlos, Arizona: Petrologic and geochemical data bearing on their petrogenesis, *Earth and Planetary Science Letters*, 38, 129–176, 1978.

Frey, F. A., Weis, D., Borisova, A. Y., et al.: Involvement of Continental Crust in the Formation of the Cretaceous Kerguelen Plateau: New Perspectives from ODP Leg 120 Sites, *Journal of Petrology*, 43, 1207–1239, 2002.

Frost, B. R., Barnes, C. G., and Collins, W. J.: A geochemical classification for granitic rocks, *Journal of Petrology*, 42, 2033–2048, 2001.

Gai, Y. S., Ma, T., Liu, L., et al.: Partial melting of HP–UHP felsic gneiss in the South Altyn Tagh reveals the rapid exhumation of a deeply subducted slab, *Lithos*, 488–489, 107835, https://doi.org/10.1016/j.lithos.2024.107835, 2024.

Gai, Y. S., Liu, L., Wang, C., et al.: Discovery of coesite in eclogite from Keqike Jianggalesayi: New evidence for ultrahigh–pressure metamorphism in South Altyn Tagh, northwestern China, *Science Bulletin*, 62, 1048–1051, 2017.

Gai, Y. S., Liu, L., Zhang, G. W., et al.: Differential exhumation of ultrahigh-pressure metamorphic terranes: A case study from South Altyn Tagh, western China, *Gondwana Research*, 104, 236–251, 2022a.

Gai, Y. S., Liu, L., Zhang, G. W., et al.: Tracking the multi–stage metamorphism and exhumation history of felsic gneisses in the South Altyn ultra–high pressure metamorphic belt, Western China, *Journal of Asian Earth Sciences*, 236, 105318, https://doi.org/10.1016/j.jseaes.2022.105318, 2022b.

Ge, R. F., Zhu, W., Wilde, S. A., and Wu, H. L.: Remnants of Eoarchean continental crust derived from a subducted proto–arc, *Science Advances*, 4, eaao3159, https://doi.org/10.1126/sciadv.aao3159, 2018.

Gehrels, G. E., Yin, A., and Wang, X. F.: Detrital–zircon geochronology of the northeastern Tibetan Plateau, *Geological Society of America Bulletin*, 115, 881–896, 2003a.

Gehrels, G. E., Yin, A., and Wang, X. F.: Magmatic history of the northeastern Tibetan Plateau, *Journal of Geophysical Research: Solid Earth*, 108, 2423, https://doi.org/10.1029/2002JB002351, 2003b.

Gerya, T. V., Stöckhert, B., and Perchuk, A. L.: Exhumation of high–pressure metamorphic rocks in a subduction channel: A numerical simulation, *Tectonics*, 21, 6–1, https://doi.org/10.1029/2001TC901048, 2002.

Hacker, B. R. and Gerya, T. V.: Paradigms, new and old, for ultrahigh-pressure tectonism, *Tectonophysics*, 603, 79–88, 2013.

Hacker, B. R., Ratschbacher, L., Webb, L., McWilliams, M. O., Ireland, T., Calvert, A., Dong, S. W., Wenk, H. R., and Chateigner, D.: Exhumation of ultrahigh-pressure continental crust in east central China: Late Triassic-Early Jurassic tectonic unroofing, *Journal of Geophysical Research: Solid Earth*, 105, 13339–13364, 2000.

Hall, P. S. and Kincaid, C.: Diapiric flow at subduction zones: A recipe for rapid transport, *Science*, 292, 2472–2475, 2001.

https://doi.org/10.5194/egusphere-2025-4830
Preprint. Discussion started: 7 October 2025

Hao, J. B., Wang, C., Zhang, J. H., Liu, L., Gai, Y. S., Li, H., Yu, Z. P., Meert, J. G., Long, X. P., Sun, X. K., and Zhang, S.: Episodic Neoproterozoic extension-related magmatism in the Altyn Tagh, NW China: implications for extension and breakup processes of Rodinia supercontinent, *International Geology Review*, 63, 1–16, 2020.

Hao, J. B., Wang, C., Zhang, S., et al.: Grenvillian evolution of the Qaidam block and its position in Rodinia constrained by U–Pb–Hf composition of detrital zircons from the Altyn Tagh, Northern Tibet, *Gondwana Research*, 122, 60–73, 2023.

Harris, N. B. W. and Inger, S.: Trace element modelling of pelite-derived granites, *Contributions to Mineralogy and Petrology*, 110, 46–56, 1992.

Hirose, K. and Kushiro, I.: Partial melting of dry peridotites at high pressures: Determination of compositions of melts segregated from peridotite using aggregates of diamond, *Earth and Planetary Science Letters*, 114, 477–489, 1993.

Kang, L., Liu, L., Wang, C., Cao, Y. T., Yang, W. Q., Wang, Y. W., and Ying, L. X.: Geochemistry and zircon U–Pb Dating of Changshagou Adakite from the South Altyn UHPM Terrane: evidence of the Partial Melting of the Lower Crust, *Acta Geologica Sinica (English Edition)*, 88, 1454–1465, 2014.

Kieffer, B., Arndt, N., Lapierre, H., et al.: Flood and Shield Basalts from Ethiopia: Magmas from the African Superswell, *Journal of Petrology*, 45, 793–834, 2004.

Ksienzyk, A. K. and Jacobs, J.: Western Australia–Kalahari (WAlahari) connection in Rodinia: Not supported by U/Pb detrital zircon data from the Maud Belt (East Antarctica) and the Northampton Complex (Western Australia), *Precambrian Research*, 259, 207–221, 2015.

Li, B. T., Massonne, H. J., Koller, F., and Zhang, J. F.: Metapelite from the high– to ultrahigh–pressure terrane of the Eastern Alps (Pohorje Mountains, Slovenia)—New pressure, temperature and time constraints on a polymetamorphic rock, *Journal of Metamorphic Geology*, 39, 695–726, 2020.

Li, X., Liu, L., Liao, X. Y., et al.: Metamorphic Evolution of Garnet Amphibolite from the Yaganbuyang Area in the South Altyn Orogen, West China: Insights from Phase Equilibria Modeling and Geochronology, *Journal of Earth Science*, 34, 640–657, 2023.

Li, Z. H.: A review on the numerical geodynamic modeling of continental subduction, collision and exhumation, *Science China Earth Sciences*, 57, 47–69, 2014.

Li, Z. H., Xu, Z. Q., and Gerya, T. V.: Flat versus steep subduction: Contrasting modes for the formation and exhumation of high– to ultrahigh–pressure rocks in continental collision zones, *Earth and Planetary Science Letters*, 301, 65–77, 2011.

Little, T. A., Hacker, B. R., Gordon, S. M., Baldwin, S. L., Fitzgerald, P. G., Ellis, S., and Korchinski, M.: Diapiric exhumation of Earth's youngest (UHP) eclogites in the gneiss domes of the D'Entrecasteaux Islands, Papua New Guinea, *Tectonophysics*, 510, 39–68, 2011.

Liu, L.: High pressure metamorphic rocks and ophiolite in Altun, and its tectonic significance, Ph.D. Thesis, Chinese Academy of Geological Sciences, 1999.

Liu, L., Che, Z. C., Wang, Y., et al.: The age of Sm–Nd isochrone of the early Paleozoic ophiolites in the Mangya area, Altyn, *Chinese Science Bulletin*, 43, 880–883, 1998.

Liu, L., Chen, D. L., Zhang, A. D., et al.: Ultrahigh pressure gneissic K–feldspar garnet clinopyroxenite in the Altyn Tagh, NW China: Evidence from clinopyroxene exsolution in garnet, *Science in China Series D: Earth Sciences*, 48, 1000–1010, 2005.

Liu, L., Sun, Y., Luo, J. H., et al.: Ultra–high pressure metamorphism of granitic gneiss in the Yinggelisayi area, Altun Mountains, NW China, *Science in China Series D: Earth Sciences*, 47, 338–346, 2004.

Liu, L., Wang, C., Cao, Y. T., et al.: Geochronology of multi–stage metamorphic events: Constraints on episodic zircon growth from the UHP eclogite in the South Altyn, NW China, *Lithos*, 136–139, 10–26, 2012.

Liu, L., Zhang, J. F., Cao, Y. T., et al.: Evidence of former stishovite in UHP eclogite from the South Altyn Tagh, western China, *Earth and Planetary Science Letters*, 484, 353–362, 2018.

Liu, L., Zhang, J. F., Green II, H. W., et al.: Evidence of former stishovite in metamorphosed sediments, implying subduction to >350 km, *Earth and Planetary Science Letters*, 263, 180–191, 2007.

Liu, Q., Tsunogae, T., Zhao, G. C., et al.: Early Cambrian high pressure/low temperature metamorphism in the southeastern Tarim craton in response to circum–Gondwana cold subduction, *Geoscience Frontiers*, 14, 101561, https://doi.org/10.1016/j.gsf.2023.101561, 2023.

Liu, Y. C., Li, Y., Liu, L. X., et al.: Neoproterozoic low–grade metagranites and metabasites in the Dabie orogen: Implications for detachment of subducted continental crust at shallow depths, *Chinese Science Bulletin*, 58, 2330–2337, 2013.

Lu, S. N., Li, H. K., Zhang, C. L., and Niu, G. H.: Geological and geochronological evidence for the Precambrian evolution of the Tarim Craton and surrounding continental fragments, *Precambrian Research*, 160, 94–107, 2008.

Ma, T., Liu, L., Gai, Y. S., et al.: Multistage metamorphism of eclogite in the South Altyn HP–UHP belt, Northwest China: Deep subduction and exhumation process of continental crust, *Journal of Metamorphic Geology*, 40, 751–787, 2022.

Ma, T., Liu, L., Gai, Y. S., Wang, C., Kang, L., Liao, X. Y., Pak, S. W., and Zhang, K.: Discovery of the high pressure granitic granulite in South Altyn and it's geological significance, *Acta Petrologica Sinica*, 34, 3643–3657, 2018.

Maierová, P., Schulmann, K., Štípská, P., Gerya, T., and Lexa, O.: Trans–lithospheric diapirism explains the presence of ultra–high pressure rocks in the European Variscides, *Communications Earth & Environment*, 2, 56, https://doi.org/10.1038/s43247-021-00122-w, 2021.

Maitre, R. W., Bateman, P., Dudek, A., et al.: A classification of igneous rocks and glossary of terms, Blackwell, Oxford, pp. 1–200, 1989.

Maniar, P. D. and Piccoli, P. M.: Tectonic discrimination of granitoids, *Geological Society of America Bulletin*, 101, 635–643, 1989.

Maruyama, S., Liou, J. G., and Terabayashi, M.: Blueschists and eclogites of the world and their exhumation, *International Geology Review*, 38, 485–594, 1996.

Massonne, H. J.: Formation of amphibole and clinozoisite–epidote in eclogite owing to fluid infiltration during exhumation in a subduction channel, *Journal of Petrology*, 53, 1969–1998, 2012.

Meng, L. T., Chen, B. L., and Zhao, N. N.: The distribution, geochronology, and geochemistry of early Paleozoic granitoid plutons in the north Altun orogenic belt, NW China: implications for the petrogenesis and tectonic evolution, *Lithos*, 268–271, 399–417, 2017.

https://doi.org/10.5194/egusphere-2025-4830
Preprint. Discussion started: 7 October 2025

Miyashiro, A. and Shido, F.: Tholeiitic and calc–alkaline series in relation to the behaviours of titanium, vanadium, chromium, and nickel, *American Journal of Science*, 275, 265–277, 1975.

Palin, R. M., Reuber, G. S., White, R. W., Kaus, B. J. P., and Weller, O. M.: Subduction metamorphism in the Himalayan ultrahigh-pressure Tso Morari massif: An integrated geodynamic and petrological modelling approach, *Earth and Planetary Science Letters*, 467, 108–119, 2017.

Pearce, J. A.: Geochemical fingerprinting of oceanic basalts with applications to ophiolite classification and the search for Archean oceanic crust, *Lithos*, 100, 14–48, https://doi.org/10.1016/j.lithos.2007.06.016, 2008.

Pearce, J. A., Harris, N. B. W., and Tindle, A. G.: Trace element discrimination diagrams for the tectonic interpretation of granitic rocks, *Journal of Petrology*, 25, 959–983, 1984.

Peng, Y. B., Yu, S. Y., Li, S. Z., et al.: Early Neoproterozoic magmatic imprints in the Altun–Qilian–Kunlun region of the Qinghai–Tibet Plateau: Response to the assembly and breakup of Rodinia supercontinent, *Earth Science Reviews*, 199, 102954, https://doi.org/10.1016/j.earscirev.2019.102954, 2019.

Peterman, E. M., Hacker, B. R., and Baxter, E. F.: Phase transformations of continental crust during subduction and exhumation: Western Gneiss Region, Norway, *European Journal of Mineralogy*, 21, 1097–1118, 2009.

Proyer, A.: The preservation of high-pressure rocks during exhumation: metagranites and metapelites, *Lithos*, 70, 183–194, 2003.

Regional Geological Survey Institute of Guangxi Zhuang Autonomous Region (RGGR): Geological Map of Washixia, Xinjiang China, Scale 1:250,000, 2003 (in Chinese).

Xinjiang Bureau of Geology and Mineral Resources (RGXR): Regional Geology of Xinjiang Uygur Autonomous Region, Geological Publishing House, Beijing, 1993 (in Chinese).

Rickwood, P. C.: Boundary lines within petrologic diagrams which use oxides of major and minor elements, *Lithos*, 22, 247–263, 1989.

Rudnick, R. L. and Gao, S.: The composition of the continental crust, In: Rudnick, R. L. (Ed.): The Crust, *Treatise on Geochemistry*, 3, Elsevier, Oxford, 1–64, 2003.

Saunders, A. D., Storey, M., Kent, R. W., et al.: Consequences of plume-lithosphere interactions, *Geological Society, London, Special Publications*, 68, 41–60, 1992.

Shervais, J. W.: Ti–V plots and the petrogenesis of modern and ophiolitic lavas, *Earth and Planetary Science Letters*, 59, 101–118, 1982.

Sizova, E., Gerya, T., and Brown, M.: Exhumation mechanisms of melt-bearing ultrahigh pressure crustal rocks during collision of spontaneously moving plates, *Journal of Metamorphic Geology*, 30, 927–955, 2012.

Štípská, P., Pitra, P., and Powell, R.: Separate or shared metamorphic histories of eclogites and surrounding rocks? An example from the Bohemian Massif, *Journal of Metamorphic Geology*, 24, 219–240, 2006.

Sun, S. S. and McDonough, W. F.: Chemical and isotopic systematics of oceanic basalts: Implications for mantle composition and processes, In: Saunders, A. D. and Norry, M. J. (Eds.): Magmatism in the Ocean Basins, *Geological Society, London, Special Publications*, 42, 313–345, 1989.

Sylvester, P. J.: Post-collisional strongly peraluminous granites, *Lithos*, 45, 29–44, 1998.

https://doi.org/10.5194/egusphere-2025-4830
Preprint. Discussion started: 7 October 2025

Wan, Y. S., Xu, Z. Q., Yan, J. S., and Zhang, J. X.: Ages and compositions of the Precambrian high-grade basement of the Qilian Terrane and its adjacent areas, *Acta Geologica Sinica*, 75, 375–384, 2001.

Wang, C., Liu, L., Yang, W. Q., Zhu, X. H., Cao, Y. T., Kang, L., Shen, S. F., Li, R., and He, S.: Provenance and ages of the Altyn complex in Altyn Tagh: implications for the early Neoproterozoic evolution of northwestern China, *Precambrian Research*, 230, 193–208, https://doi.org/10.1016/j.precamres.2013.02.003, 2013.

Wang, C. M., Tang, H. S., Zheng, Y., Dong, L. H., and Qu, X.: Early paleozoic magmatism and metallogeny related to proto-tethys subduction: insights from volcanic rocks in the northeastern Altyn mountains, NW China, *Gondwana Research*, 75, 134–153, 2019.

Wang, K., Plank, T., Walker, J. D., et al.: A mantle melting profile across the Basin and Range, SW USA, *Journal of Geophysical Research: Solid Earth*, 107, ECV 5-1-ECV 5-21, https://doi.org/10.1029/2001JB000209, 2002.

Warren, C. J., Beaumont, C., and Jamieson, R. A.: Formation and exhumation of ultra-high-pressure rocks during continental collision: Role of detachment in the subduction channel, *Geochemistry, Geophysics, Geosystems*, 9, Q04019, https://doi.org/10.1029/2007GC001839, 2008.

Whitney, D. L. and Evans, B. W.: Abbreviations for names of rock-forming minerals, *American Mineralogist*, 95, 185–187, 2010.

Whitney, D. L., Teyssier, C., Kruckenberg, S. C., Morgan, V. L., and Iredale, L. J.: High-pressure-low-temperature metamorphism of metasedimentary rocks, southern Menderes Massif, western Turkey, *Lithos*, 101, 218–232, 2008.

Winchester, J. A. and Floyd, P. A.: Geochemical magma type discrimination: Application to altered and metamorphosed igneous rocks, *Earth and Planetary Science Letters*, 28, 459–469, 1976.

Wright, J. B.: A simple alkalinity ratio and its application to questions of non-orogenic granite genesis, *Geological Magazine*, 106, 370–384, 1969.

Wu, C. L., Yao, S. Z., Zeng, L. S., Yang, J. S., Wooden, J. L., Chen, S. Y., and Mazadab, F. K.: Bashikaogong-Shimierbulake granitic complex, north Altun, NW China: geochemistry and zircon SHRIMP ages, *Science in China Series D: Earth Sciences*, 50, 1755–1773, https://doi.org/10.1007/s11430-007-0123-8, 2007.

Yao, J. L., Cawood, P. A., Zhao, G. C., Han, Y. G., Xia, X. P., Liu, Q., et al.: Mariana type ophiolites constrain establishment of modern plate tectonic regime during Gondwana assembly, *Nature Communications*, 12, 4189, https://doi.org/10.1038/s41467-021-24422-1, 2021.

Yin, A., Manning, C. E., Lovera, O., Menold, C. A., Chen, X., and Gehrels, G. E.: Early Paleozoic tectonic and thermomechanical evolution of ultrahigh-pressure (UHP) metamorphic rocks in the northern Tibetan Plateau, Northwest China, *International Geology Review*, 49, 681–716, 2007.

Young, D. J. and Kylander-Clark, A. R. C.: Does continental crust transform during eclogite facies metamorphism?, *Journal of Metamorphic Geology*, 33, 331–357, 2015.

Yu, S. Y., Zhang, J. X., Del Real, P. G., Zhao, X. L., Hou, K. J., Gong, J. H., and Li, Y. S.: The Grenvillian orogeny in the Altun-Qilian-North Qaidam mountain belts of northern Tibet

https://doi.org/10.5194/egusphere-2025-4830
Preprint. Discussion started: 7 October 2025

Plateau: constraints from geochemical and zircon U-Pb age and Hf isotopic study of magmatic rocks, *Journal of Asian Earth Sciences*, 73, 372–395, 2013.

Zhang, J. X., Mattinson, C. G., Meng, F. C., et al.: An early Paleozoic HP/HT granulite-garnet peridotite association in the South Altyn Tagh, NW China: P-T history and U-Pb geochronology, *Journal of Metamorphic Geology*, 23, 491–510, 2005.

Zhang, J. X., Meng, F. C., Yu, S. Y., Chen, W., and Chen, S. Y.: Ar-Ar geochronology of blueschist and eclogite in the North Altyn Tagh HP/LT metamorphic belt and their regional tectonic implication, *Geology in China*, 34, 558–564, 2007 (in Chinese with English abstract).

Zhang, J. X., Yu, S. Y., Li, Y. S., et al.: Subduction, accretion and closure of Proto-Tethyan Ocean: early Paleozoic accretion/collision orogeny in the Altun-Qilian-north Qaidam orogenic system, *Acta Petrologica Sinica*, 31, 3531–3554, 2015 (in Chinese with English abstract).

Zhang, J. X., Yu, S. Y., and Mattinson, C. G.: Early Paleozoic polyphase metamorphism in northern Tibet, China, *Gondwana Research*, 41, 267–289, 2017.

Zhang, J. X., Zhang, Z. M., Xu, Z. Q., et al.: Petrology and geochronology of eclogites from the western segment of the Altyn Tagh, northwestern China, *Lithos*, 56, 187–206, 2001.

Zheng, Y. F.: Metamorphic chemical geodynamics in continental subduction zones, *Chemical Geology*, 328, 5–48, 2012.

Zheng, Y. F., Zhou, J. B., Wu, Y. B., and Xie, Z.: Low-grade metamorphic rocks in the Dabie-Sulu orogenic belt: A passive-margin accretionary wedge deformed during continent subduction, *International Geology Review*, 47, 851–871, 2005.

Zhou, J. B.: Accretionary complex: Geological records from oceanic subduction to continental deep subduction, *Science China Earth Sciences*, 63, 1868–1883, https://doi.org/10.1007/s11430-019-9652-6, 2020.

Zhou, J. B., Cheng, R. H., Liu, P. J., and Liu, J. H.: Tectonic implications of the low-grade metamorphic rocks for the subduction of a continental plate in the Dabie-Sulu orogen, *Advances in Earth Science*, 19, 736–742, 2004 (in Chinese with English abstract).

Zhu, X. H., Cao, Y. T., Liu, L., Wang, C., and Chen, D. L.: P-T path and geochronology of high pressure granitic granulite from Danshuiquan area in Altyn Tagh, *Acta Petrologica Sinica*, 30, 3717–3728, 2014 (in Chinese with English abstract).